Electronic Supplementary Material (ESI) for Journal of Materials Chemistry C.

Supporting Information

Multiple Stimuli Responsive Afterglow in Carbazole-Attributed Coordination Polymers

Jia-Yi Zhuang, Zhong-Hao Wang, Yan-Ting Huang, Qiang-Sheng Zhang and Mei Pan*

MOE Laboratory of Bioinorganic and Synthetic Chemistry, Lehn Institute of Functional Materials, IGCME, GBRCE for Functional Molecular Engineering, School of Chemistry, Sun Yat-Sen University, Guangzhou 510006, P. R. China

Experimental Section

All reagents of analytical grades were obtained from commercial sources and used without further purification. Fourier transform infrared (FT-IR) spectra were recorded in the 4000-400 cm^{-1} region using KBr pellets and a Nicolet/Nexus-670 FT-IR spectrometer. A Mini-Pellet Press of Specac is used to compress the samples. Normal powder X-ray diffraction patterns (PXRD) were determined with a Rigaku Miniflex600 diffractometer (Bragg-Brentano geometry, Cu $K_{\alpha 1}$ radiation, λ = 1.54056 Å). The in-situ temperature-variable powder X-ray diffraction patterns were determined with a Rigaku SmartLab diffractometer (Bragg-Brentano geometry, Cu $K_{\alpha 1}$ radiation, λ = 1.54056 Å). ^{1}H and ^{13}C NMR spectra were recorded on a Bruker AVANCE III spectrometer (400 MHz). Thermogravimetric analysis (TGA) was performed on a NETZSCH TG209 system in nitrogen gas under 1 atm at a heating rate of 10 °C/min. The photoluminescence spectrum and time-gated emission spectra were tested on the Edinburgh FLS 980 and FLS 1000 PL spectrometer. The steady-state photoluminescence spectra were obtained by using Xe-900 450W ozone-free xenon lamp as the light source, and the delayed spectra were obtained by using single wavelength laser or μF920 microsecond pulsed flash lamp as the light source. Time dependent single photon counting technology and multi-channel scanning technology were used for decay lifetime acquisition. The photoluminescence quantum yields were measured on a Hamamatsu C9920-02G absolute photoluminescence quantum yield measurement system. UV-Vis absorption spectra were recorded on a Shimadzu UV-3600 spectrometer. Elementary analysis was performed on a Vario EL element analyzer. The long persistent luminescence (LPL) spectra were recorded on an Ocean Optics spectrophotometer (QE65 Pro) using 365 nm (3 W), 385 nm (1 W), 405 nm (1 W) and 450 nm (1 W) UV light from the flashlight as excitation light source. The measurements were carried out in high-velocity scanning mode of QE65 Pro with integration time of 20 ms and scanning time of 20 s. The videos for long persistent luminescence were recorded by Canon EOS 5D Mark IV camera with 365, 385, 405,

450 nm UV flashlight as excitation light source. All optical experiments were carried out in the air.

Synthetic Procedures

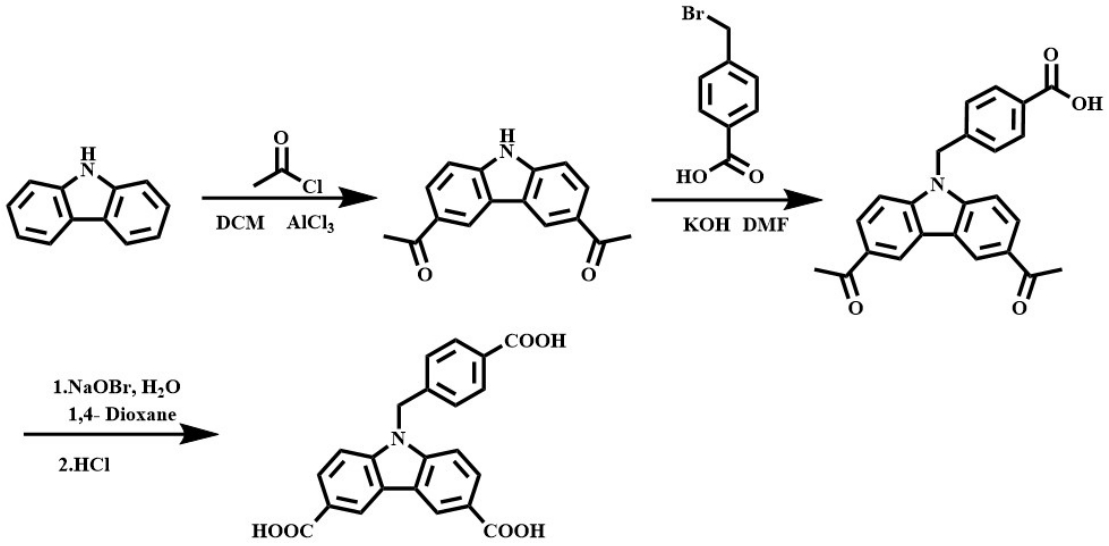

Scheme S1. Synthetic route of ligand L.

1,1'-(9H-carbazole-3,6-diyl)bis(ethan-1-one) (1)

Acetyl chloride (21.3 ml, 299 mmol) and aluminum chloride (23.9 g, 179.4 mmol) were dispersed in 200 ml of methylene chloride and stirred at 0 ℃ for 30 min. Carbazole (10 g, 59.8 mmol) was then added to the mixture, stirred for 10 minutes, and then slowly raised to room temperature for 3 hours. When the reaction is over, place the mixture in an ice bath and stir in a small amount of water. Stop adding water when the system stops boiling and precipitates gray solid. Strain solids and rinse with plenty of water. The solid is dissolved in ethanol, and the excess water is added to precipitate the gray solid. The solids are filtered and cleaned again with plenty of water. (14 g, yield 93.6%). ^{1}H NMR (DMSO-d_6, 400 MHz, ppm): δ 12.11 (1H, s); 9.04 (2H, s); 8.07 (2H, d); 7.63 (2H, d); 2.70 (6H, s). ESI calcd for $C_{16}H_{13}NO_2^+$ (MH^+) 251.09 found 251.0899. Elemental analysis: Calcd for $C_{16}H_{13}NO_2 \cdot 11H_2O$: C, 42.76%; H, 7.79%; N, 3.12%. Found: C, 42.65 %; H, 6.71 %; N, 2.47 %.

4-((3,6-diacetyl-9H-carbazol-9-yl)methyl)benzoic acid (2)

Dissolve 3, 6-diformylcarbazole (2.16 g, 8.62 mmol) in 50 ml DMF, add 500 mg

NaH, stir at room temperature for 30 min; When no gas was produced, slowly add p-bromomethylbenzoic acid (1.85 g, 8.62 mmol) and stir at room temperature for 12 h; At the end of the reaction, filter cake was washed with DMF for several times, then washed with ethanol, filtrate was collected, dilute hydrochloric acid was added to the filtrate, white solid was precipitated, and ethanol was washed and filtered. (2.66 g, 80% yield). ^{1}H NMR (DMSO-d_6, 400 MHz, ppm): δ 9.10 (2H, s); 8.11 (2H, d); 7.86 (2H, d); 7.84 (2H, d); 7.24 (2H, d); 5.88 (2H, s); 2.71 (6H, s). ESI calcd for $C_{24}H_{19}NO_4^+$ (MH^+) 385.13 found 385.1274. Elemental analysis: Calcd. for $C_{24}H_{19}NO_4$: C, 74.79 %; H, 4.97 %; N, 3.63 %. Found: C, 76.46 %; H, 7.24 %; N, 2.58 %.

9-(4-carboxybenzyl)-9H-carbazole-3,6-dicarboxylic acid (L)

Dissolve 4-((3, 6-diacetyl-9h-carbazol-9-yl)methyl)benzoic acid in 42 ml dioxane. Take a separate flask and place it at 0 ℃, add 42 ml water, 10 g sodium hydroxide, and 5 ml liquid bromine. Stir at 0 ℃ for half an hour. Drop the solution from the flask into another flask and heat the reflux at 100 ° C for 12 h. At the end of the reaction, it was cooled to room temperature, saturated sodium sulfite solution was added, after filtration, the filtrate was acidified with dilute hydrochloric acid, filtered, and washed solid with water and ethanol several times. (1.50 g, 77% yield). ^{1}H NMR (DMSO-d_6, 400 MHz, ppm): δ 8.92 (2H, s); 8.08 (2H, d); 7.86 (2H, d); 7.76 (2H, d); 7.26 (2H, d); 5.88 (2H, s). ESI calcd for $C_{22}H_{15}NO_6^+$ (MH^+) 389.09 found 389.0859. Elemental analysis: Calcd. for $C_{22}H_{15}NO_6 \cdot 5H_2O$: C, 55.11%; H, 5.22 %; N, 2.92 %. Found: C, 57.51 %; H, 4.18 %; N, 2.24 %.

Synthesis of LIFM-ZJY-1 ($\{Cd(L)(DMF)(H_2O)\}_n$)

$Cd(CH_3COO)_2 \cdot 2.5H_2O$ (26 mg, 0.1 mmol) and ligand (38 mg, 0.1 mmol) were dissolved in a mixture of 6 mL DMF/H_2O (5:1, v/v) and transferred to a 20 mL glass bottle. After 10 minutes of ultrasound, the glass bottle was placed in an oven at 120 ℃ for 72 hours, and then the system was slowly and naturally cooled to room temperature to obtain crystals. After washing with fresh DMF for 3 times, the product was dried and named LIFM-ZJY-1. Elemental analysis: Calcd. for $C_{25}H_{21}CdN_2O_8 \cdot 7H_2O$: C, 41.04 %;

H, 4.79 %; N, 3.83 %. Found: C, 41.22 %; H, 4.01 %; N, 3.55 %.

Synthesis of LIFM-ZJY-2 ($\{Zn(L)(DMF)(H_2O)\}_n$)

$Zn(NO_3)_2 \cdot 6H_2O$ (29 mg, 0.1 mmol) and ligand (19 mg, 0.05mmol) were dissolved in a mixture of 5 mL DMF/H2O (3:2, v/v) and transferred to a 20 mL glass bottle. After 10 minutes of ultrasound, the glass bottle was placed in an oven at 110 ℃ for 72 hours, and then the system was slowly and naturally cooled to room temperature to obtain crystals. After washing with fresh DMF for 3 times, the product was dried and named LIFM-ZJY-2. Elemental analysis: Calcd. for $C_{25}H_{21}ZnN_2O_8 \cdot 5H_2O$: C, 48.54 %; H, 5.01 %; N, 4.53 %. Found: C, 49.14 %; H, 4.63 %; N, 3.90 %.

X-ray Single Crystal Structural Analysis

Single-crystal X-ray diffraction data for all samples were collected on a Rigaku Oxford SuperNova X-RAY diffractometer system equipped with a Cu sealed tube (λ = 1.54178 Å) at 50 kV and 0.80 mA. The structure was solved by direct methods, and refined by full-matrix least-square methods with the SHELXL-2014 program package and OLEX2 program.[1,2] All hydrogen atoms were located in calculated positions and refined anisotropically. The crystallographic data for all compounds were listed in Table S1. The single crystal data have been deposited in the Cambridge Crystallographic Data Center (See Table S1 for CCDC numbers).

Calculation Methods

The structural optimization and electronic structure natures of **L** at the level of B3LYP-D3(BJ)/6-311G (d) have been calculated with Gaussian 09 program package.[3] Time-dependent density functional theory (TD-DFT) calculations were performed based on the optimized molecular structure. Spin-orbital coupling matrix elements (SOCME, ξ) were investigated by ORCA program based on the TD-DFT results.[4] The Hirshfeld surfaces, decomposed fingerprint plots and the unoccupied spaces (free volumes) were calculated and mapped using CrystalExplorer 21.5 package.[5] The frontier orbitals were carried out by Multiwfn program and visuallized by VMD.[6,7]

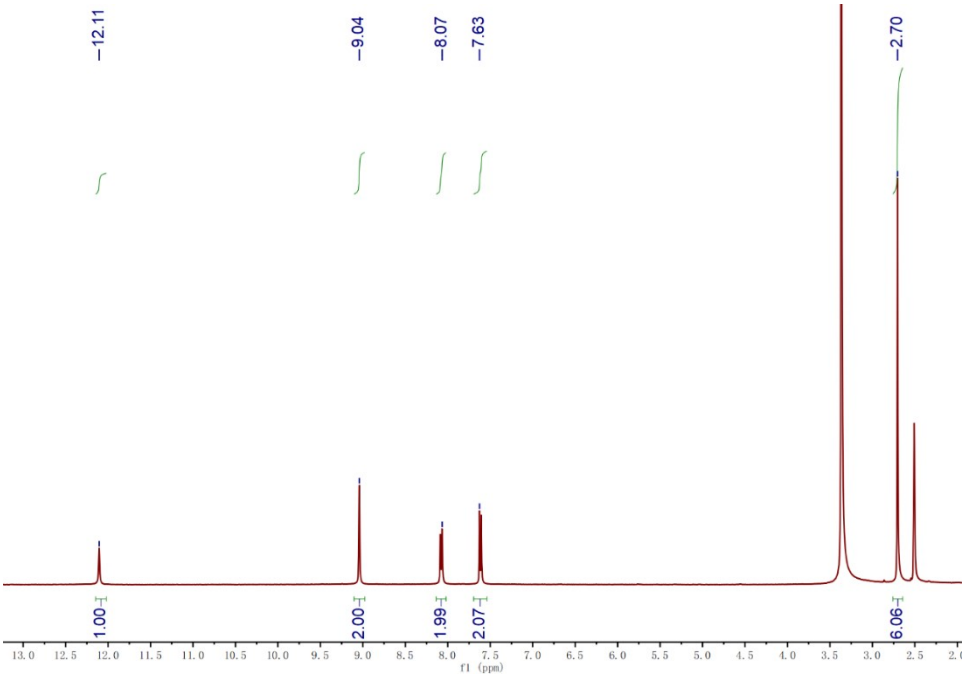

Figure S1. ^{1}H NMR spectrum of compound 1 in DMSO-d_6.

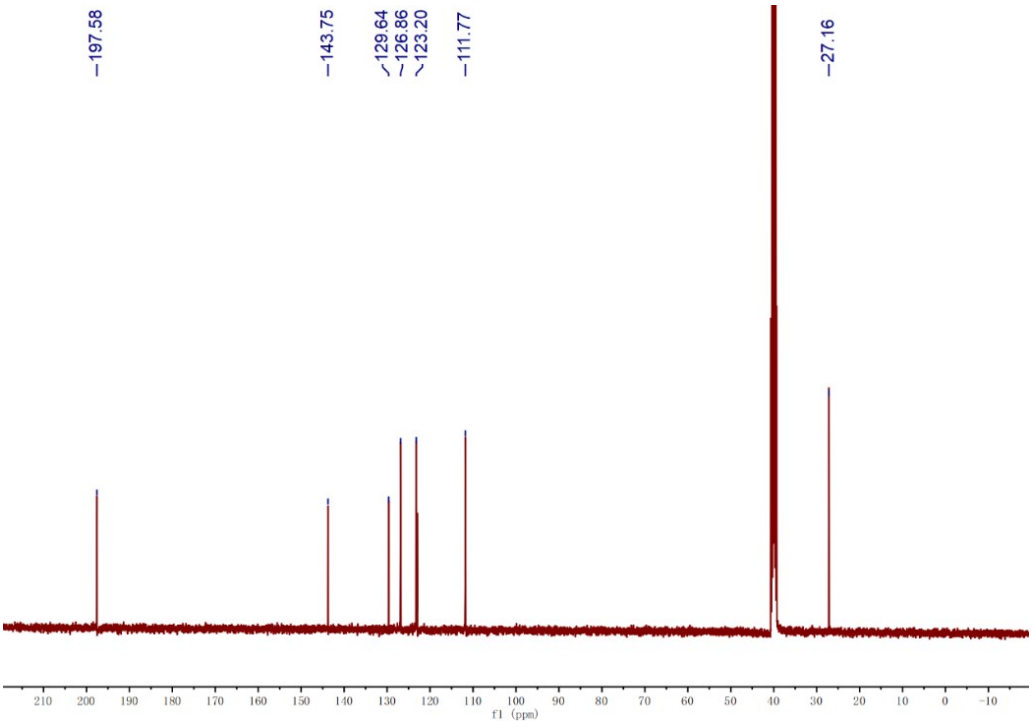

Figure S2. ^{13}C NMR spectrum of compound 1 in DMSO-d_6.

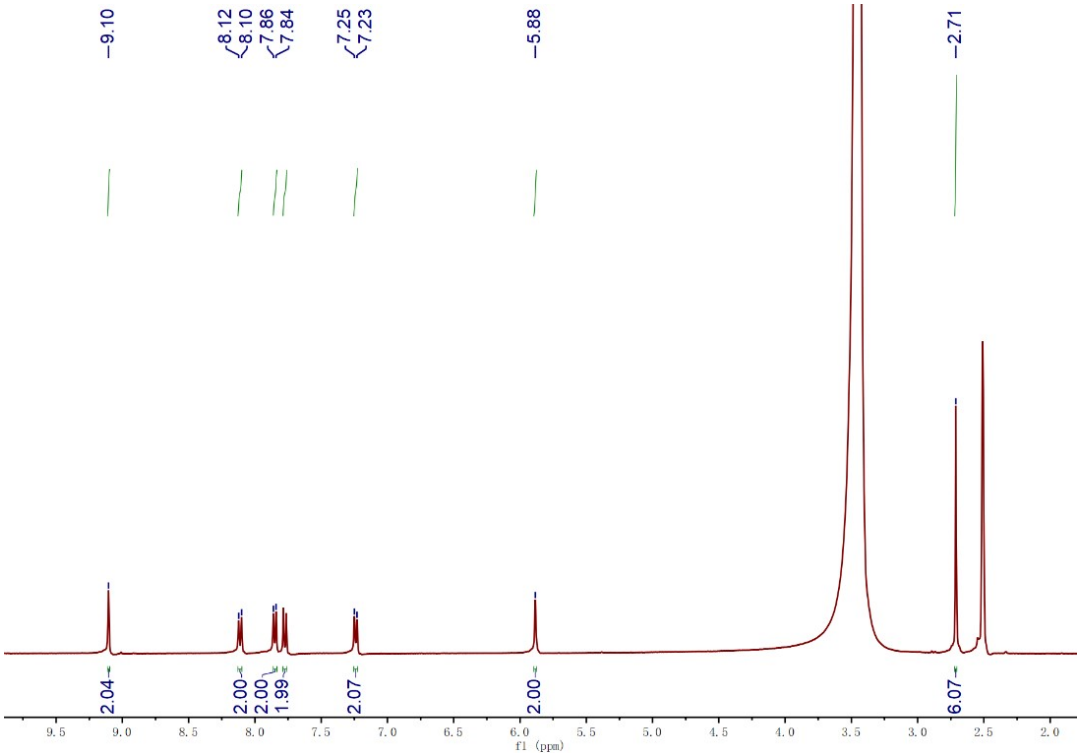

Figure S3. ^{1}H NMR spectrum of compound 2 in DMSO-d_6.

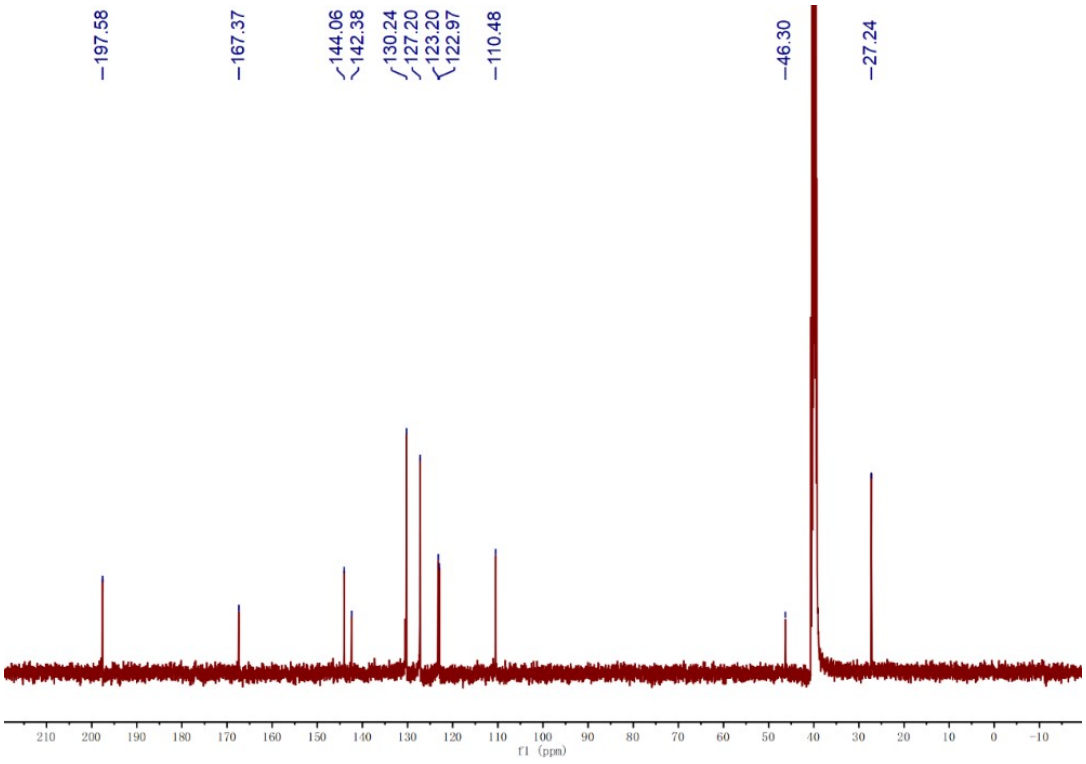

Figure S4. ^{13}C NMR spectrum of compound 2 in DMSO-d_6.

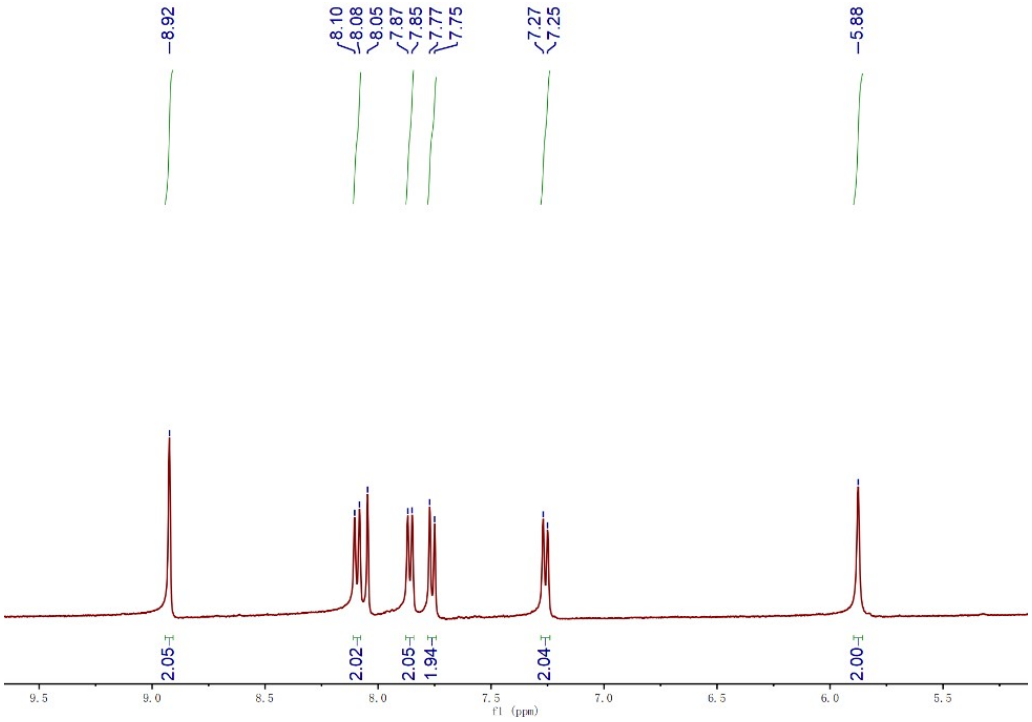

Figure S5. ^{1}H NMR spectrum of compound L in DMSO-d_6.

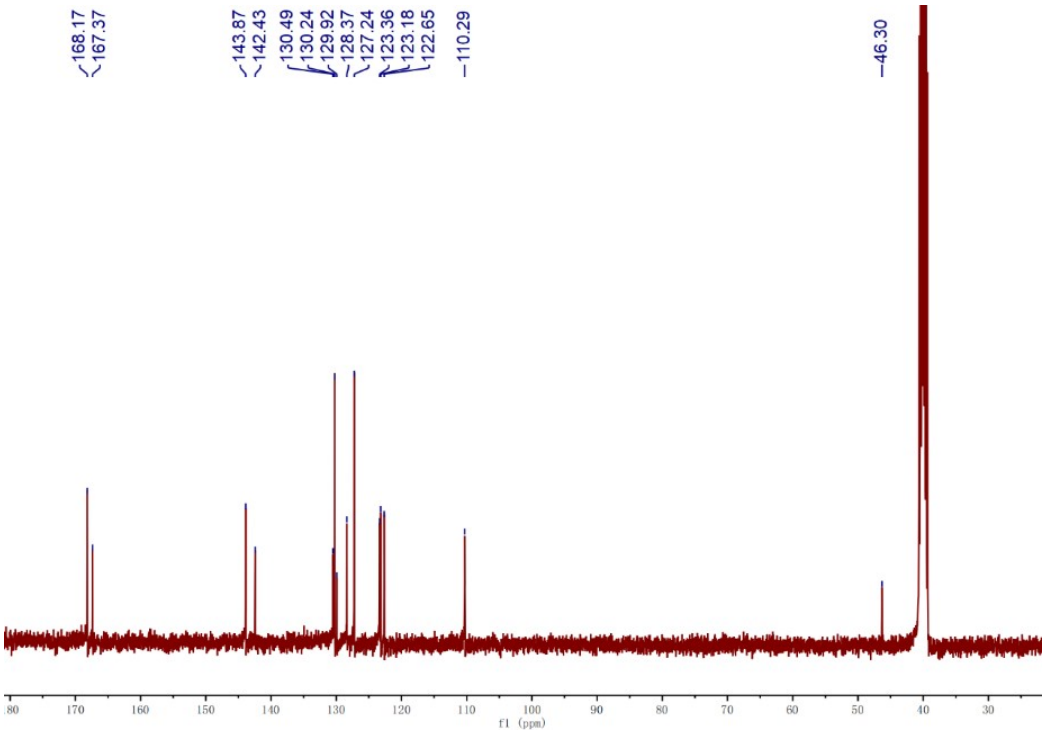

Figure S6. ^{13}C NMR spectrum of compound L in DMSO-d_6.

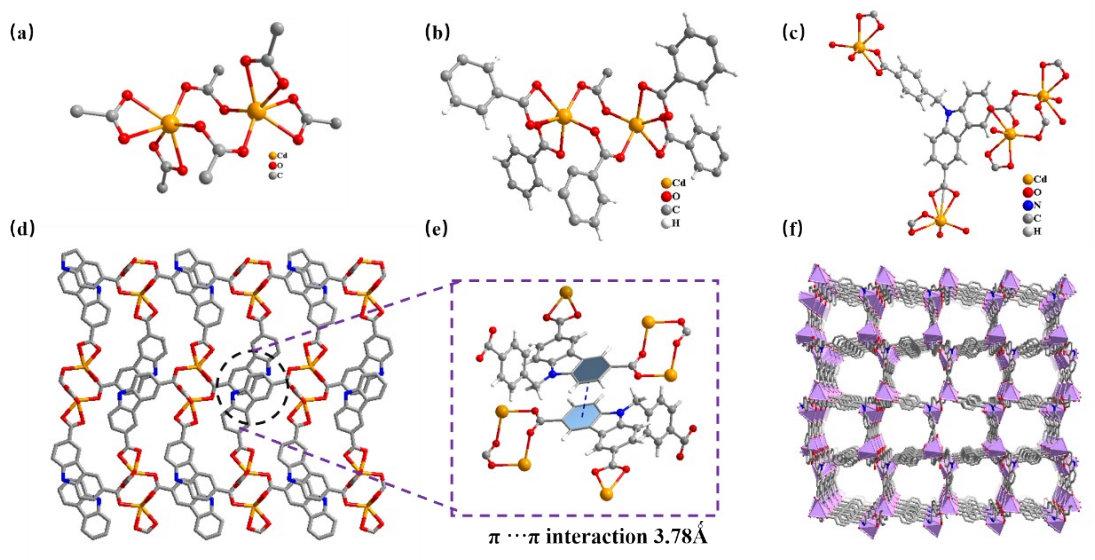

Figure S7. Crystal structure of **LIFM-ZJY-1** (a) Coordination environment of Cd^{2+}. (b) Bridging modes of adjacent Cd-O polyhedron (color indication: Cd: orange; O, red; C, grey; N, blue and H, white). (c) Coordination environment of L; (d-f) Two and three dimensional structure of **LIFM-ZJY-1**; (e) The weak π-π interactions between ligand molecules.

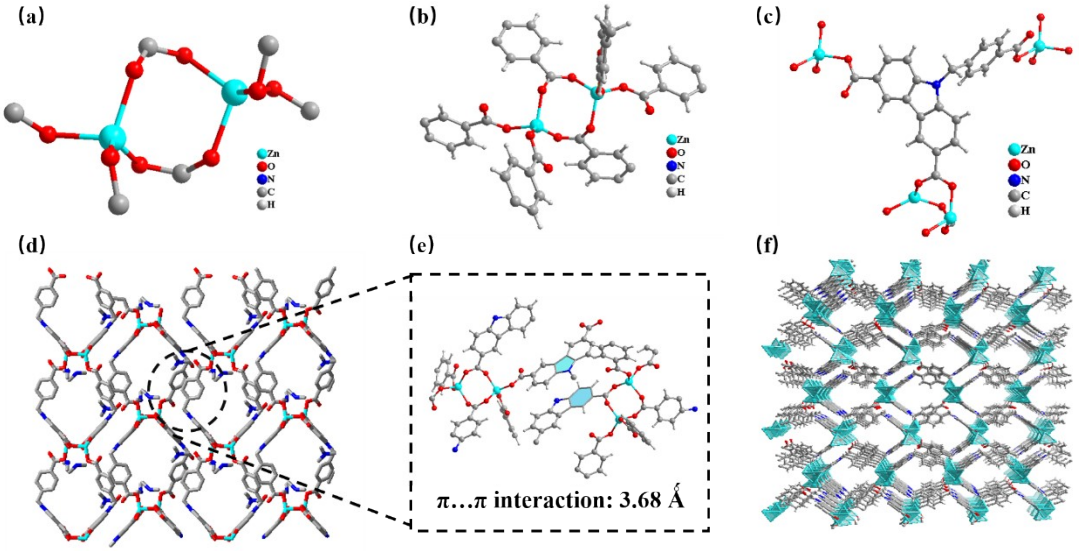

Figure S8. Crystal structure of **LIFM-ZJY-2** (a) Coordination environment of Zn^{2+}. (b) Bridging modes of adjacent Zn-O polyhedron (color indication: Zn: blue; O, red; C, grey; N, blue and H, white). (c) Coordination environment of L; (d-f) Two and three dimensional structure of **LIFM-ZJY-2**; (e) The weak π-π interactions between ligand molecules.

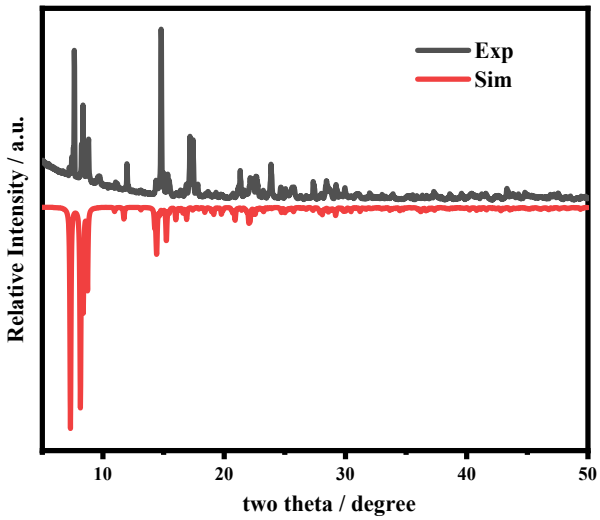

Figure S9. The powder X-ray diffraction patterns of **LIFM-ZJY-1.**

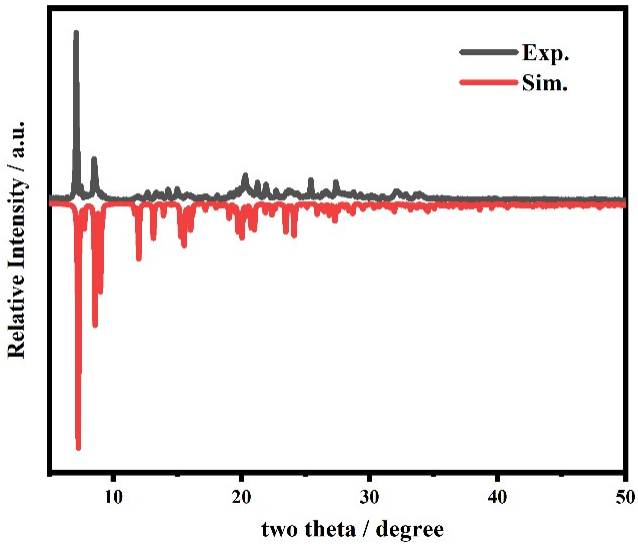

Figure S10. The powder X-ray diffraction patterns of **LIFM-ZJY-2**.

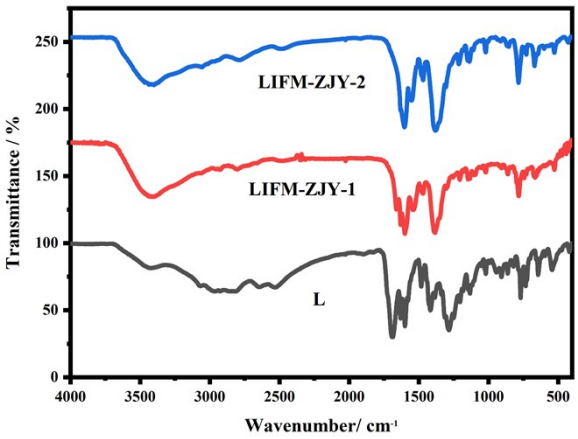

Figure S11. Fourier transform infrared (FT-IR) spectroscopy of L, **LIFM-ZJY-1**,

LIFM-ZJY-2.

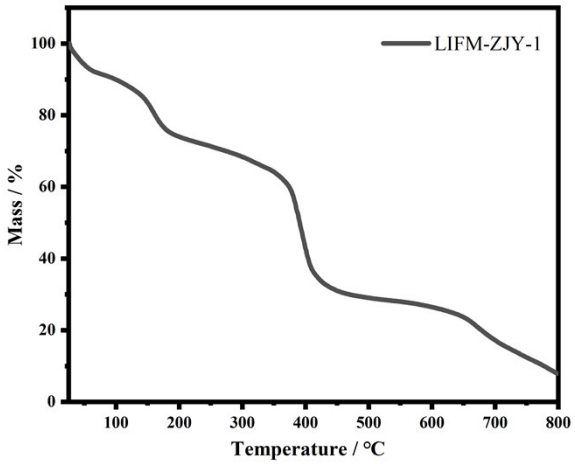

Figure S12. Thermogravimetric analysis (TGA) of **LIFM-ZJY-1** in nitrogen gas.

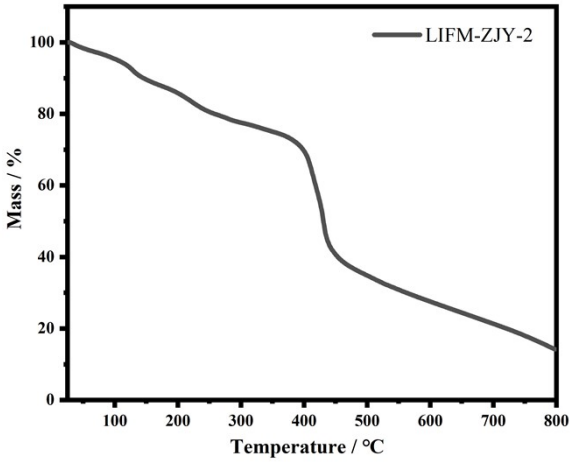

Figure S13. Thermogravimetric analysis (TGA) of **LIFM-ZJY-2** in nitrogen gas.

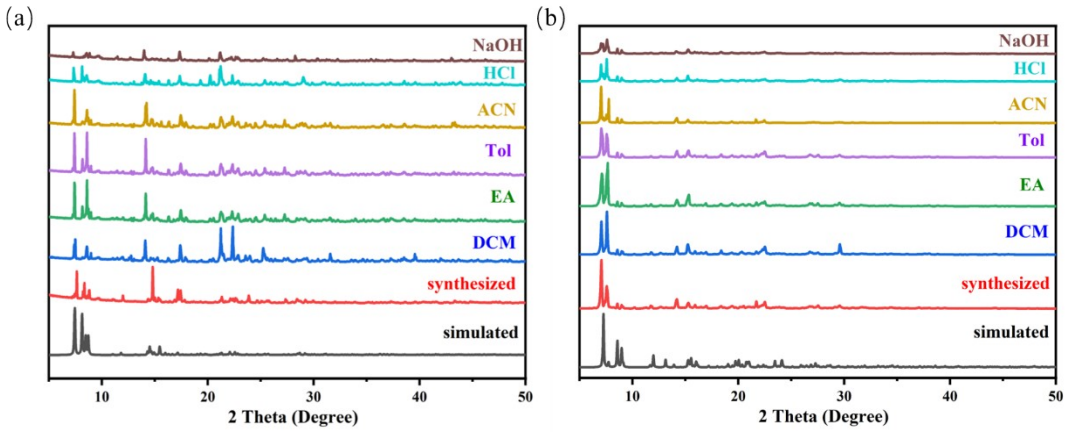

Figure S14. (a) PXRD patterns of **LIFM-ZJY-1** after soaking in different solvents for

one day (HCl aqueous solution: pH = 2, NaOH aqueous solution: pH = 12). (b) PXRD patterns of **LIFM-ZJY-2** after soaking in different solvents for one day (HCl aqueous solution: pH = 2, NaOH aqueous solution: pH = 12).

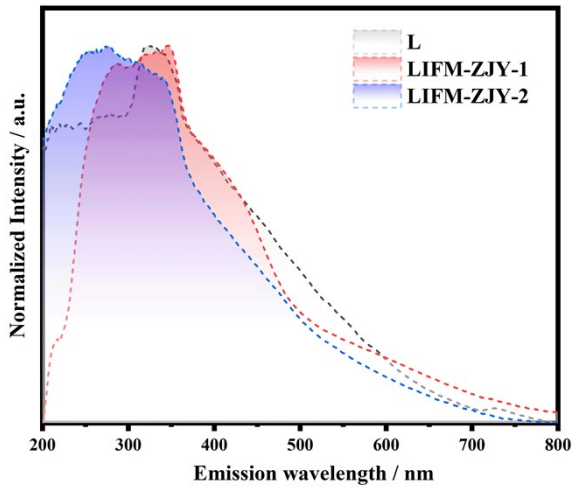

Figure S15. The UV-Vis absorption spectrum of L, **LIFM-ZJY-1**, **LIFM-ZJY-2** in solid state.

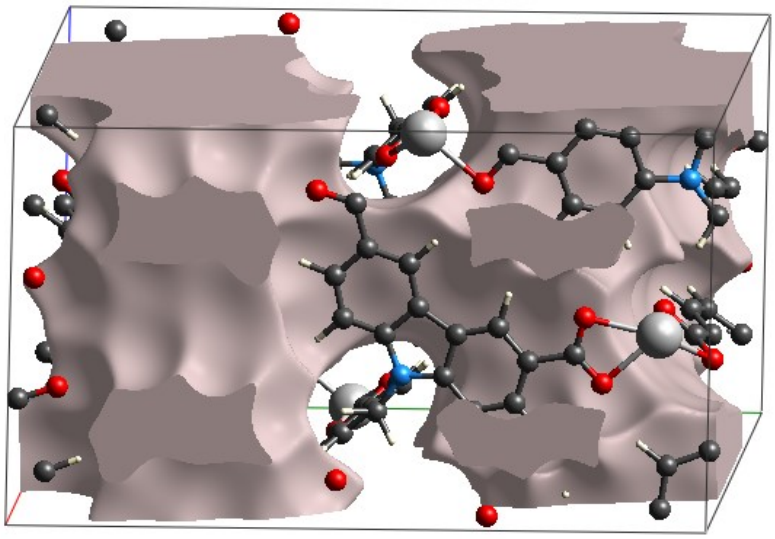

Figure S16. The calculated free volume region in the single crystal cell of **LIFM-ZJY-1** (isovalue = 0.002 e·au^{-3}).

V_{free} / Å^3	V_{total} / Å^3	Percentage
1579.48	3167.93	49.8%

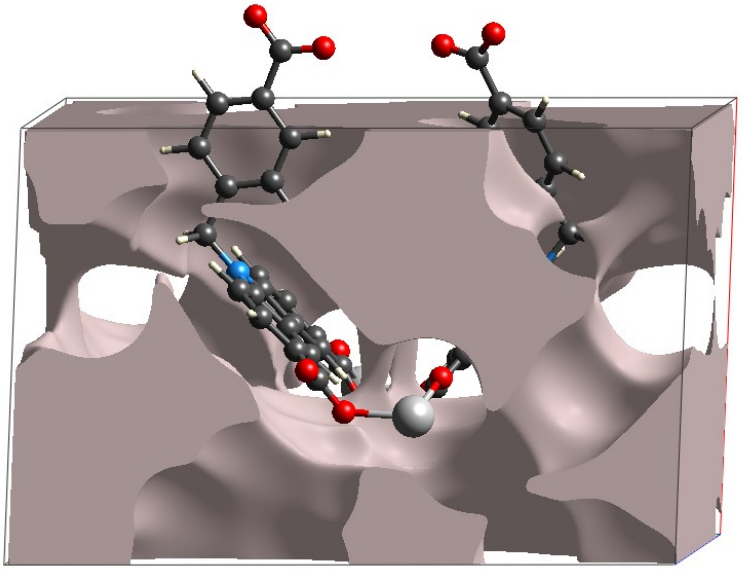

Figure S17. The calculated free volume region in the single crystal cell of **LIFM-ZJY-2** (isovalue = 0.002 e·au^{-3}).

V_{free} / Å^3	V_{total} / Å^3	Percentage
1586.04	3176.75	49.9%

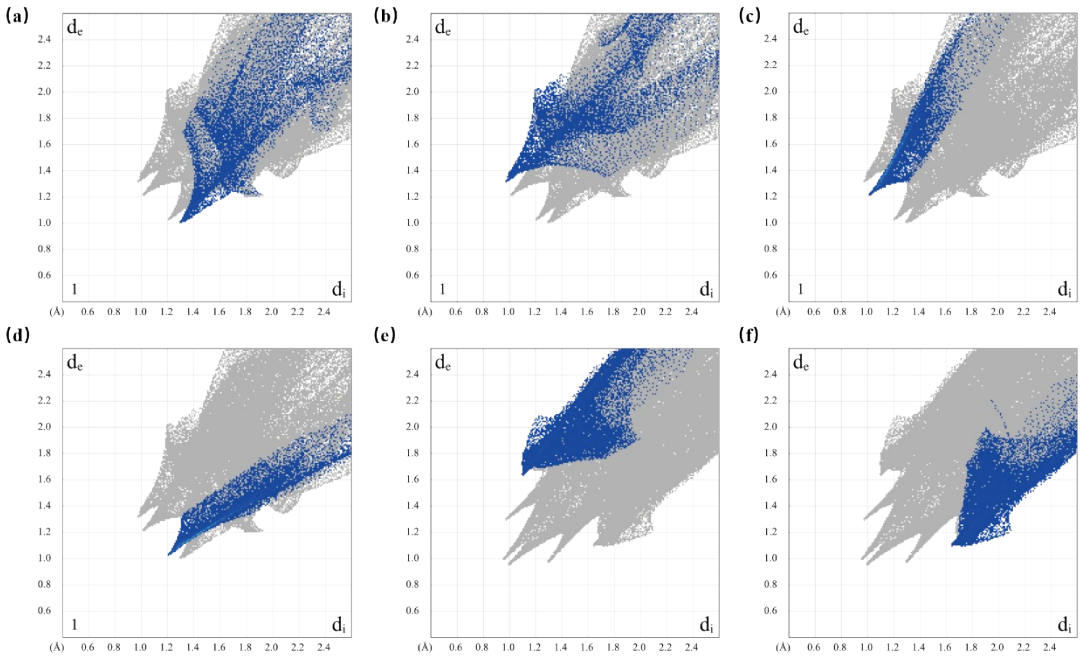

Figure S18. Hirshfeld surface analysis of **LIFM-ZJY-1** mapped with the parameter d_{norm} along with 2D fingerprint plots with (a) O-H interaction. (b) H-O interaction. (c) O-Cd interaction. (d) Cd-O interaction. (e) H-C interaction. (f) C-H interaction.

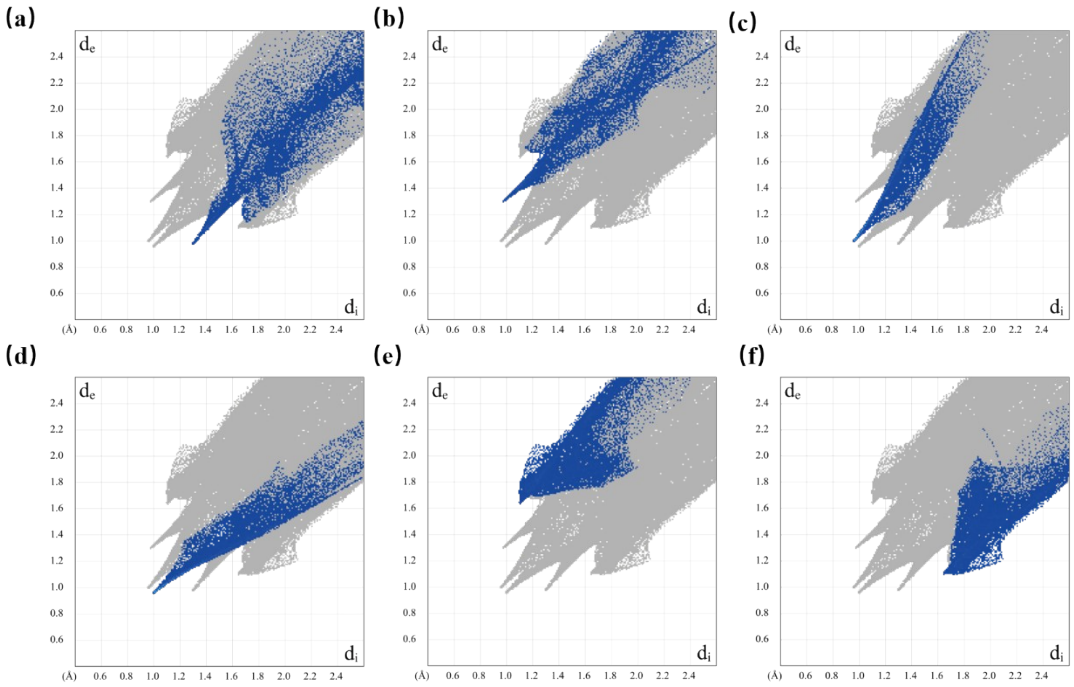

Figure S19. Hirshfeld surface analysis of **LIFM-ZJY-2** mapped with the parameter d_{norm} along with 2D fingerprint plots with (a) O-H interaction. (b) H-O interaction. (c) O-Zn interaction. (d) Zn -O interaction. (e) H-C interaction. (f) C-H interaction.

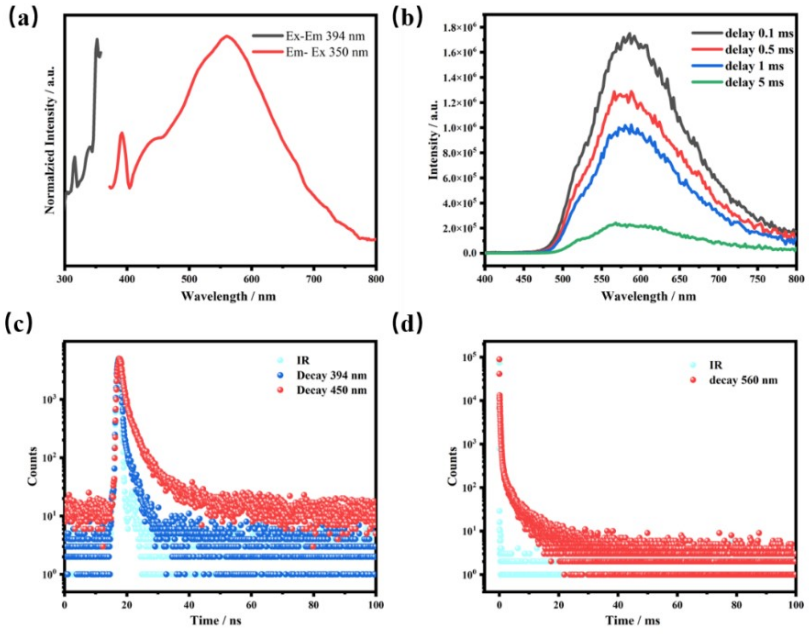

Figure S20. (a) The excitation and emission spectra of L at room temperature. (b) The time resolved delayed emission spectra of L at room temperature. (c) The time-resolved fluorescence emission decay curves of L at room temperature. (d) The time-resolved phosphorescence emission decay curves of L at room temperature.

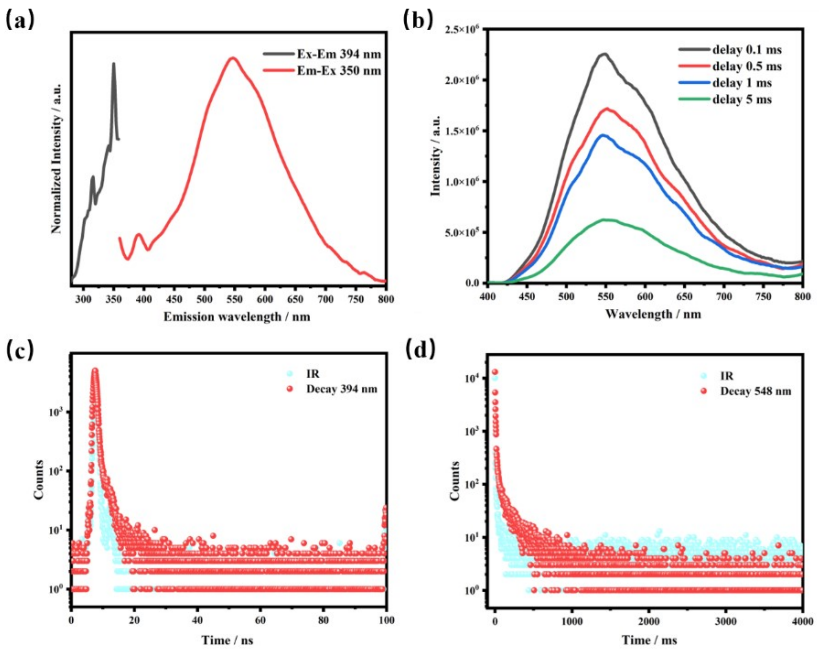

Figure S21. (a) The excitation and emission spectra of L at 77 K. (b) The time resolved delayed emission spectra of L at 77 K. (c) The time-resolved fluorescence emission decay curves of L at 77 K. (d) The time-resolved phosphorescence emission decay curves of L at 77 K.

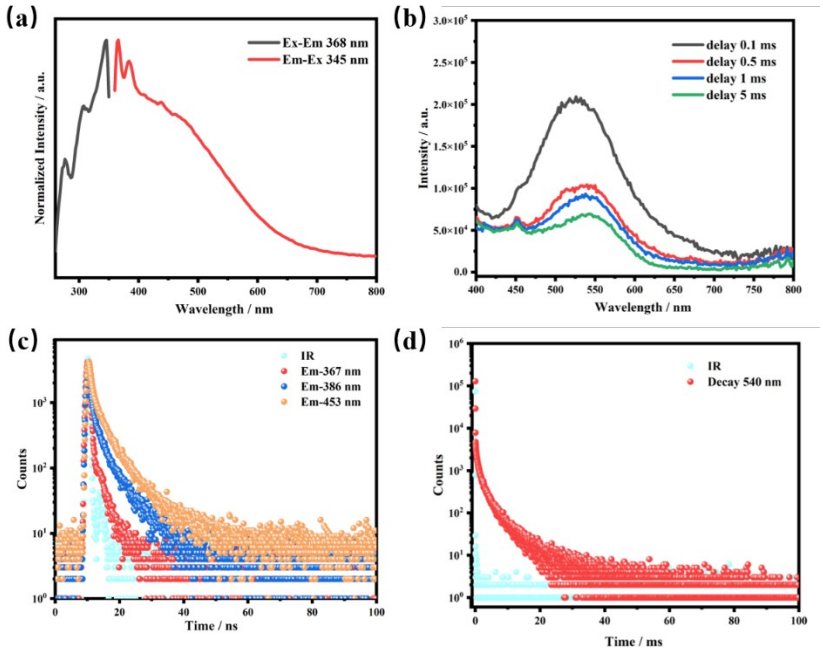

Figure S22. (a) The excitation and emission spectra of **LIFM-ZJY-1** at RT. (b) The time resolved delayed emission spectra of **LIFM-ZJY-1** at RT. (c) The time-resolved fluorescence emission decay curves of **LIFM-ZJY-1** at RT. (d) The time-resolved phosphorescence emission decay curves of **LIFM-ZJY-1** at RT.

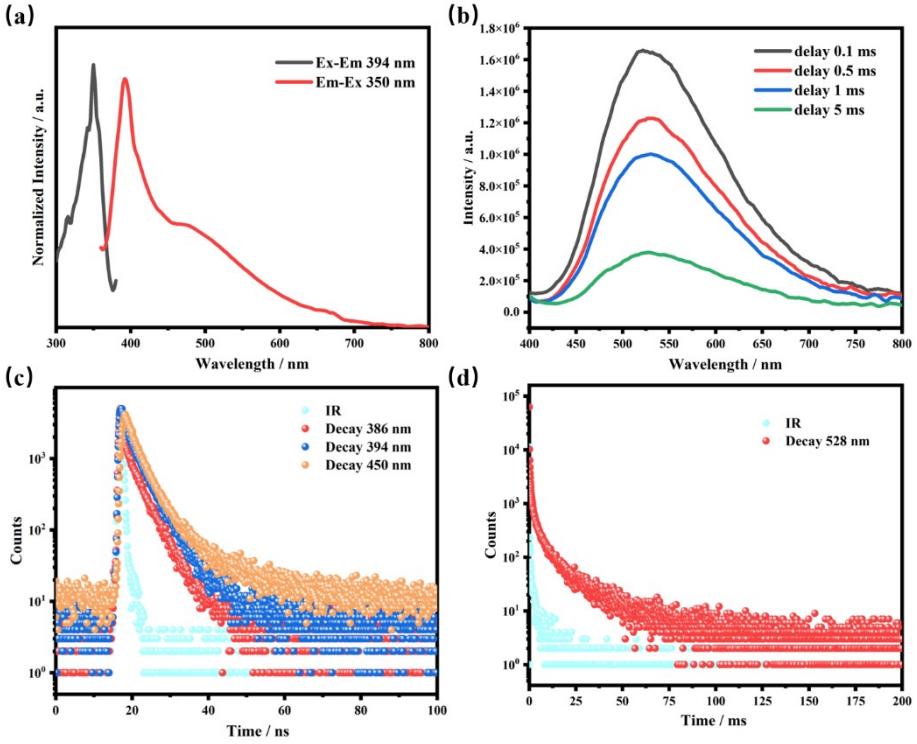

Figure S23. (a) The excitation and emission spectra of **LIFM-ZJY-2** at RT. (b) The time resolved delayed emission spectra of **LIFM-ZJY-2** at RT. (c) The time-resolved fluorescence emission decay curves of **LIFM-ZJY-2** at RT. (d) The time-resolved phosphorescence emission decay curves of **LIFM-ZJY-2** at RT.

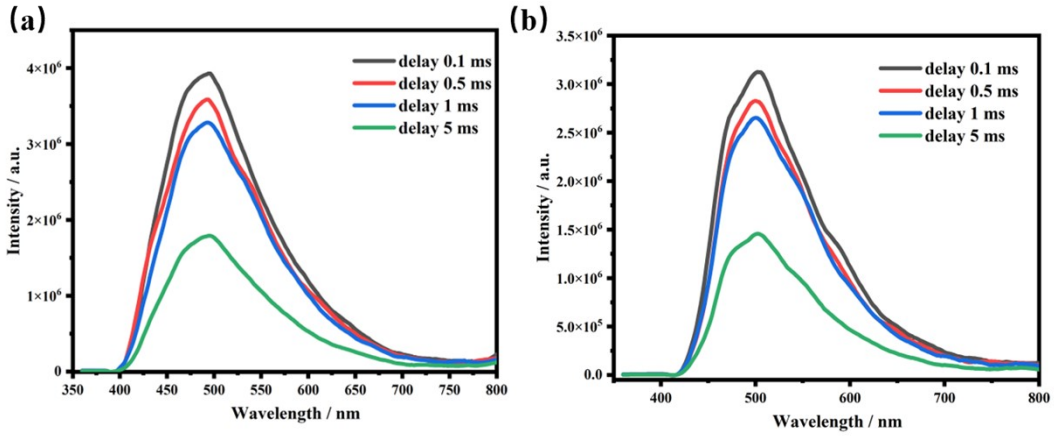

Figure S24. (a) The delayed emission spectrum of **LIFM-ZJY-1** at 77 K. (b)The delayed emission spectrum of **LIFM-ZJY-2** at 77 K.

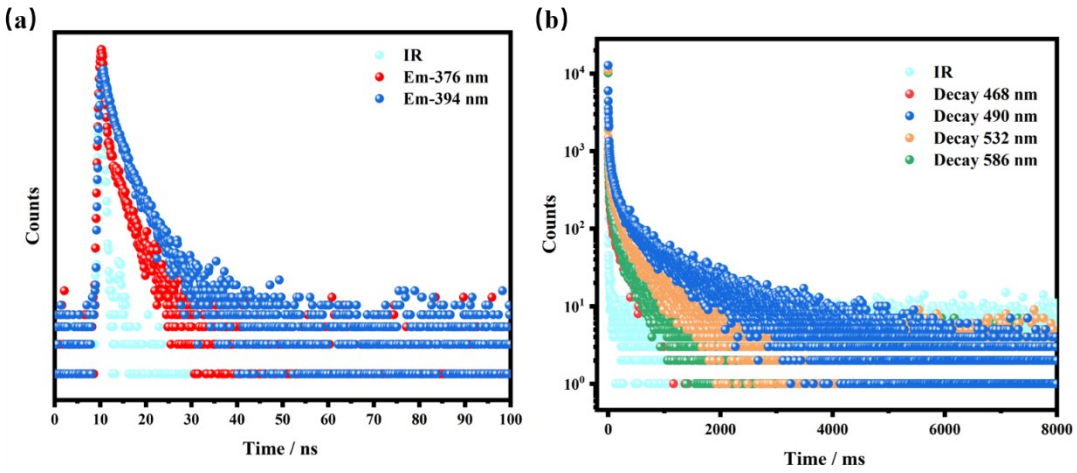

Figure S25. (a) The time-resolved fluorescence emission decay curves of **LIFM-ZJY-1** at 77 K. (b) The time-resolved phosphorescence emission decay curves of **LIFM-ZJY-1** at 77 K.

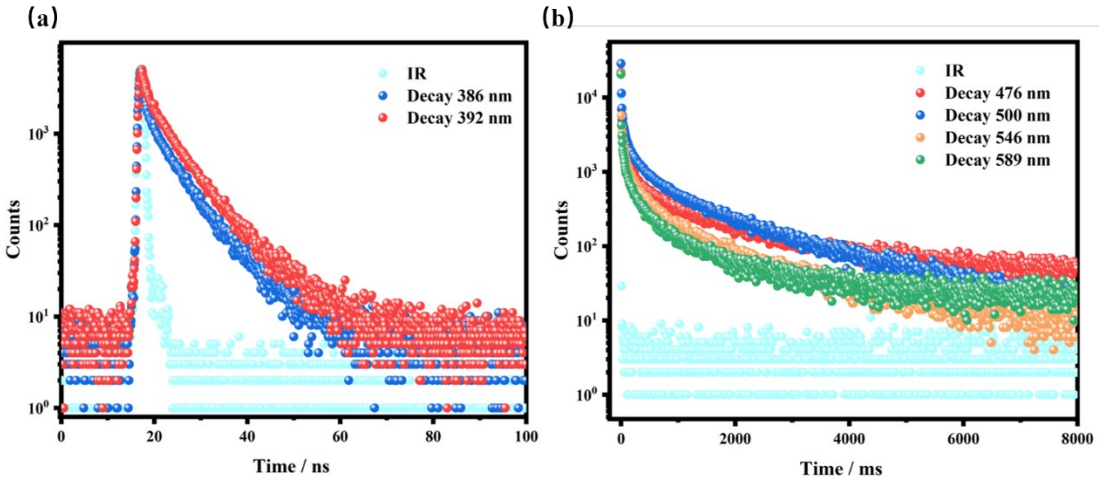

Figure S26. (a) The time-resolved fluorescence emission decay curves of **LIFM-ZJY-2** at 77 K. (b) The time-resolved phosphorescence emission decay curves of **LIFM-ZJY-2** at 77 K.

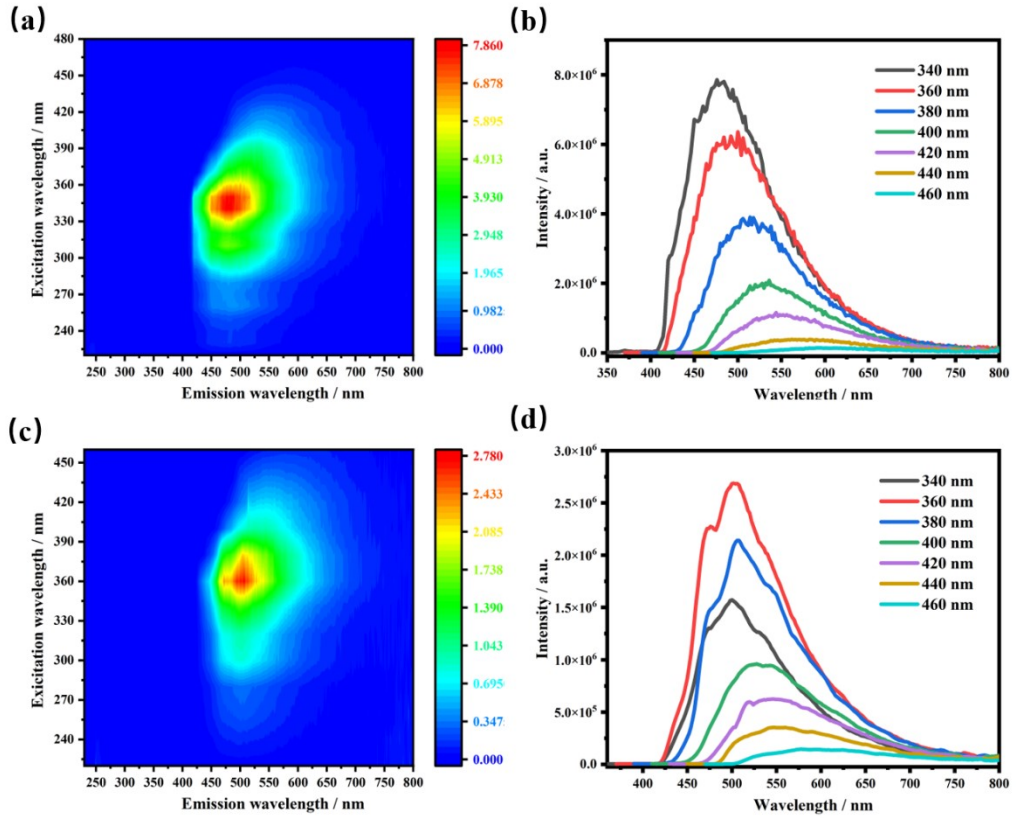

Figure S27. (a) Excitation–delayed emission mapping of **LIFM-ZJY-1** at 77 K. (b) The delayed spectrum of **LIFM-ZJY-1** at different excitation wavelength. (c) Excitation–delayed emission mapping of **LIFM-ZJY-2** at 77 K. (d) The delayed spectrum of **LIFM-ZJY-2** at different excitation wavelength.

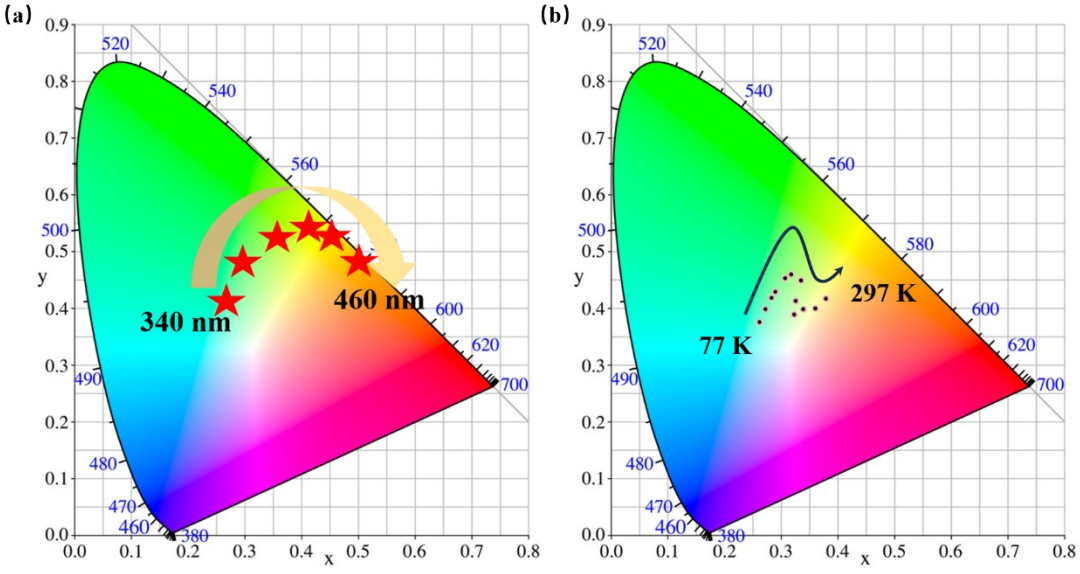

Figure S28. (a) The excitation wavelength-dependent phosphorescence CIE coordinate diagram of **LIFM-ZJY-2**. (b) The temperature-dependent phosphorescence CIE coordinate diagram of **LIFM-ZJY-1** at different temperatures.

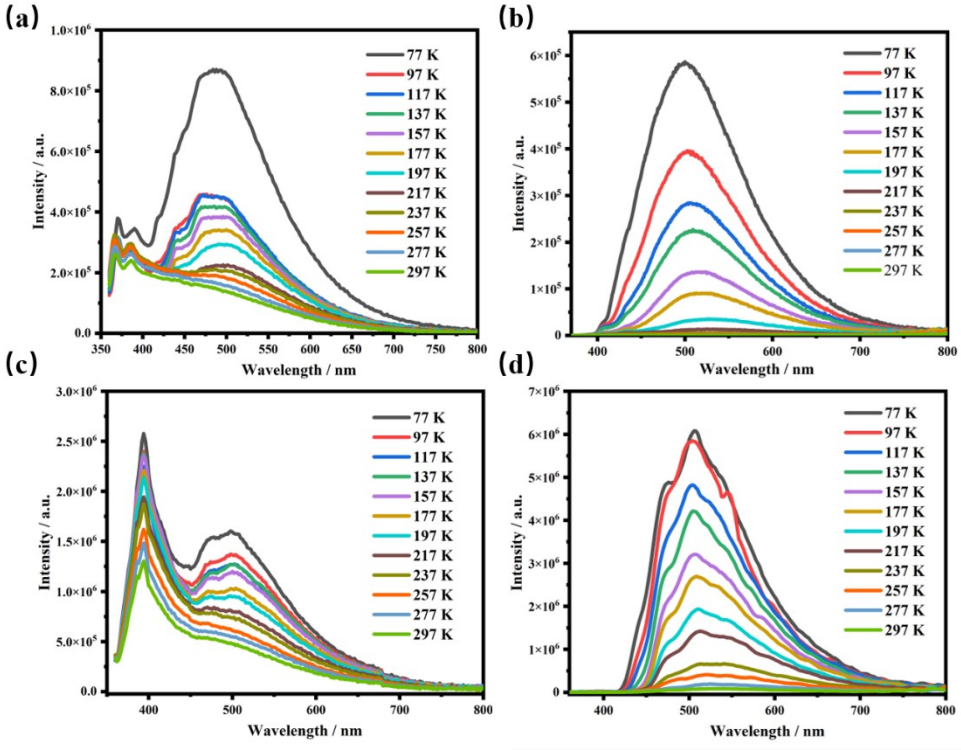

Figure S29. (a) The temperature-dependent prompt emission spectrum of **LIFM-ZJY-1**. (b) The temperature-dependent delayed emission spectrum of **LIFM-ZJY-1**. (c) The temperature-dependent prompt emission spectrum of **LIFM-ZJY-2**. (d) The temperature-dependent delayed emission spectrum of **LIFM-ZJY-2**.

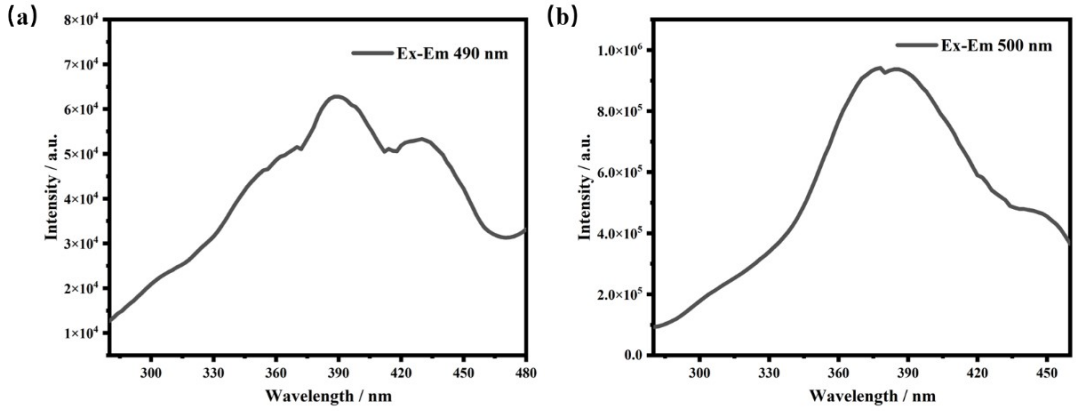

Figure S30. (a) The excitation spectra at 490 nm of **LIFM-ZJY-1** at 77 K. (b) The excitation spectra at 500 nm of **LIFM-ZJY-2** at 77 K.

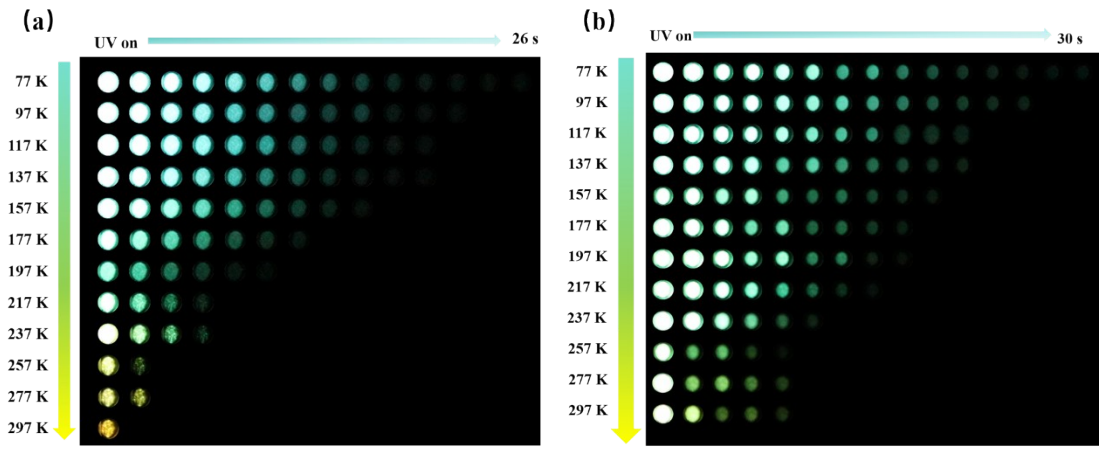

Figure S31. LPL photographs of (a) **LIFM-ZJY-1** and (b) **LIFM-ZJY-2** at different time intervals and different temperature after the removal of 385 nm UV light.

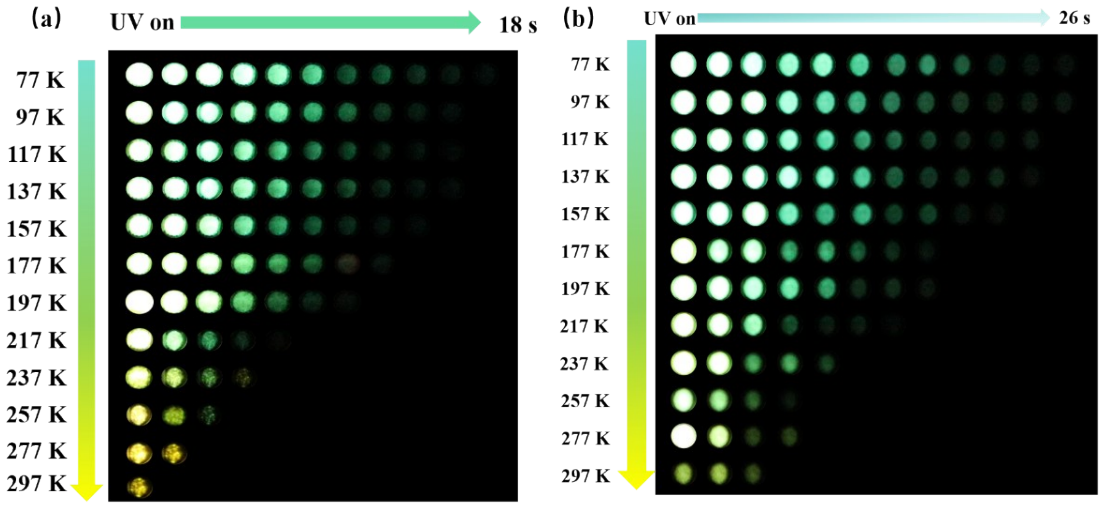

Figure S32. LPL photographs of (a) **LIFM-ZJY-1** and (b) **LIFM-ZJY-2** at different time intervals and different temperature after the removal of 405 nm UV light.

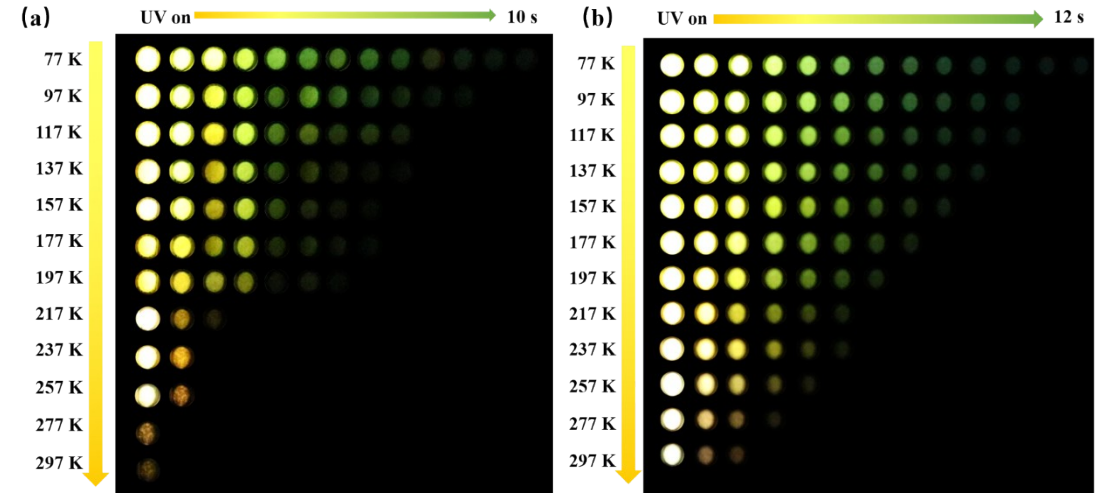

Figure S33. LPL photographs of (a) **LIFM-ZJY-1** and (b) **LIFM-ZJY-2** at different time intervals and different temperature after the removal of 450 nm UV light.

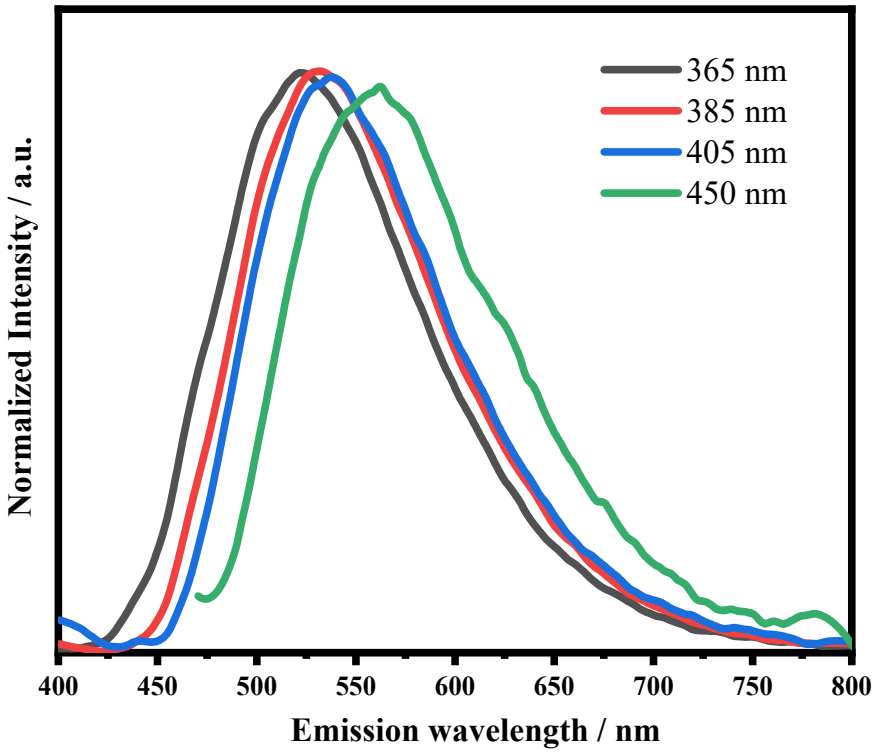

Figure S34. LPL spectra of **LIFM-ZJY-1** at 77 K at different excitation wavelength.

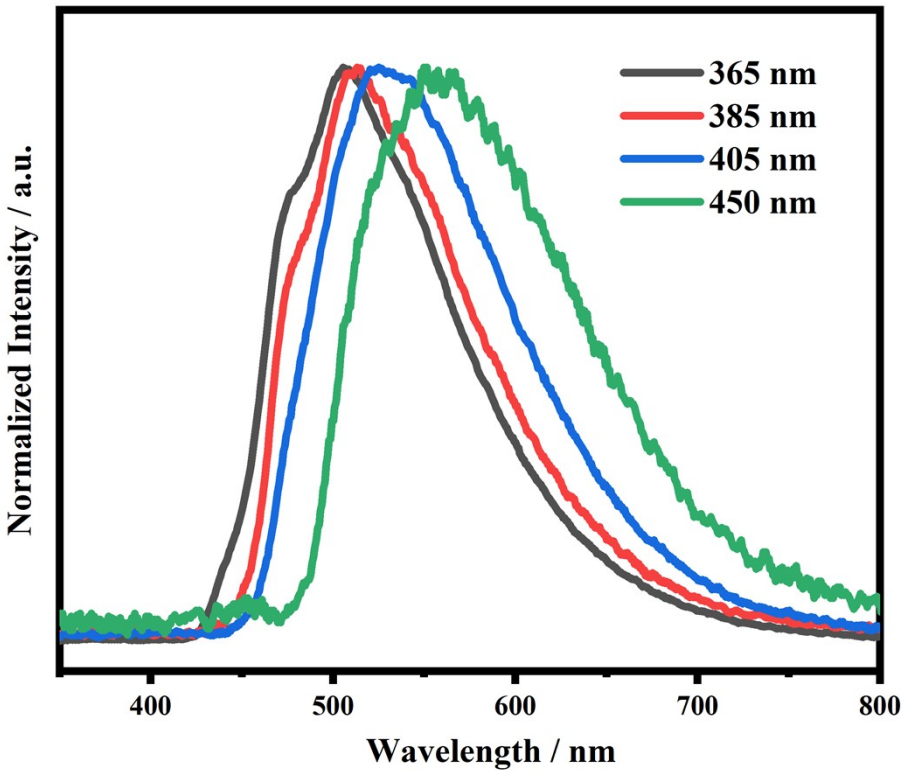

Figure S35. LPL spectra of **LIFM-ZJY-2** at 77 K at different excitation wavelength.

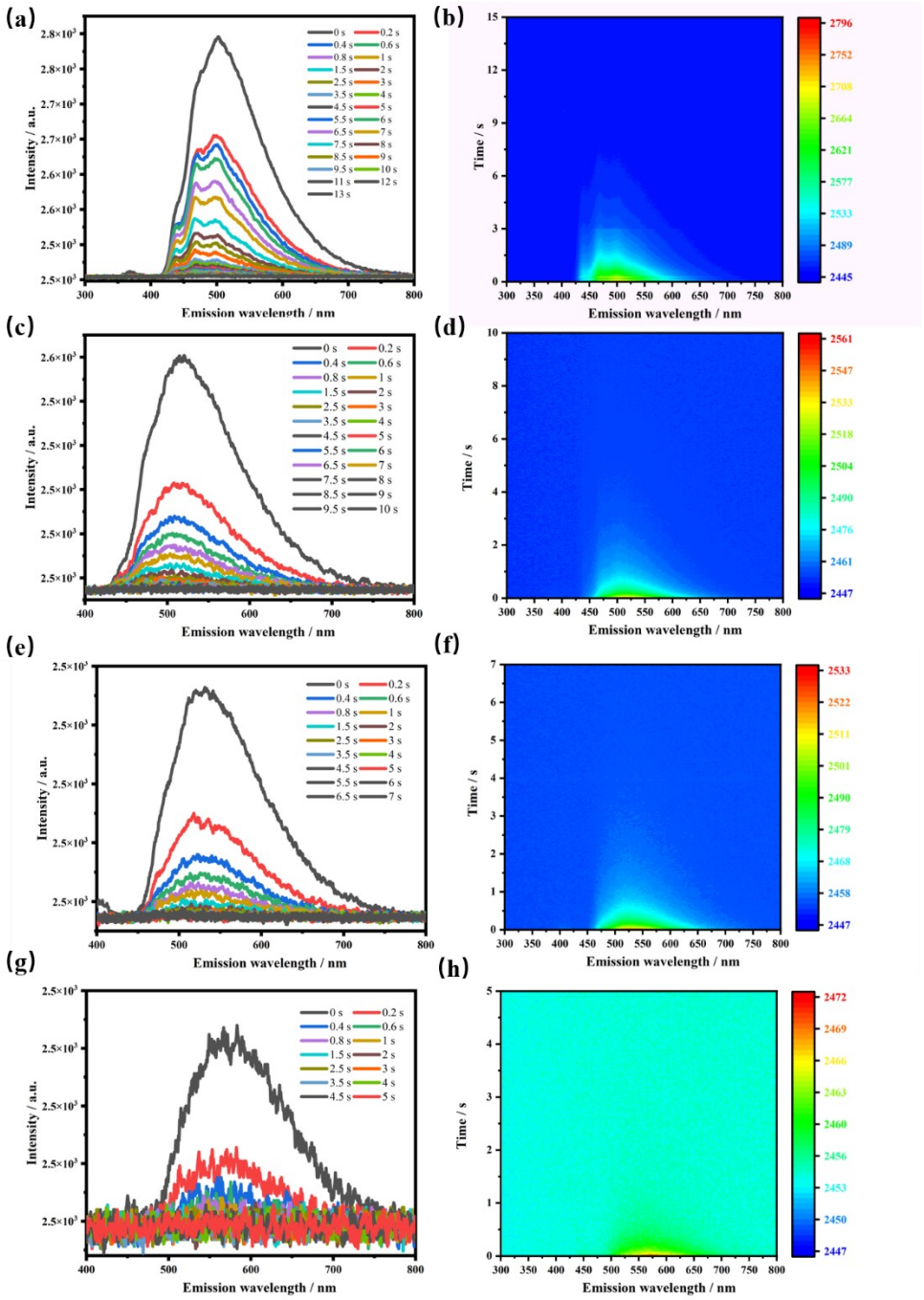

Figure S36. (a, b) The afterglow spectrums of **LIFM-ZJY-1** at different time intervals after excitation by 365 nm at room temperature. (c, d) The afterglow spectrums of **LIFM-ZJY-1** at different time intervals after excitation by 385 nm at room temperature. (e, f) The afterglow spectrums of **LIFM-ZJY-1** at different time intervals after excitation by 405 nm at room temperature. (g, h) The afterglow spectrums of **LIFM-ZJY-1** at different time intervals after excitation by 450 nm at room

temperature.

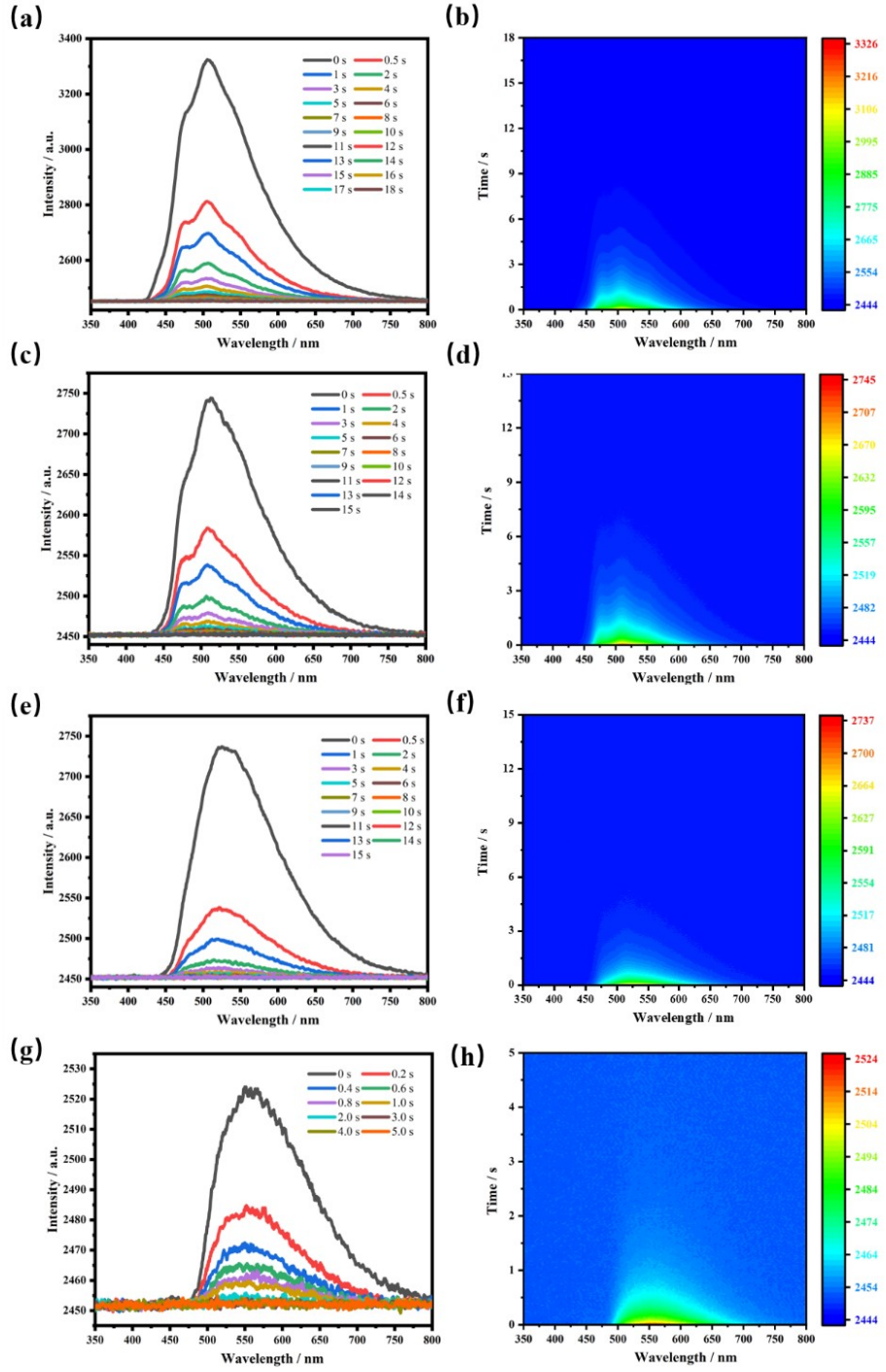

Figure S37. (a, b) The afterglow spectrums of **LIFM-ZJY-2** at different time intervals after excitation by 365 nm at room temperature. (c, d) The afterglow spectrums of **LIFM-ZJY-2** at different time intervals after excitation by 385 nm at room temperature. (e, f) The afterglow spectrums of **LIFM-ZJY-2** at different time intervals after excitation by 405 nm at room temperature. (g, h) The afterglow spectrums of

LIFM-ZJY-2 at different time intervals after excitation by 450 nm at room temperature.

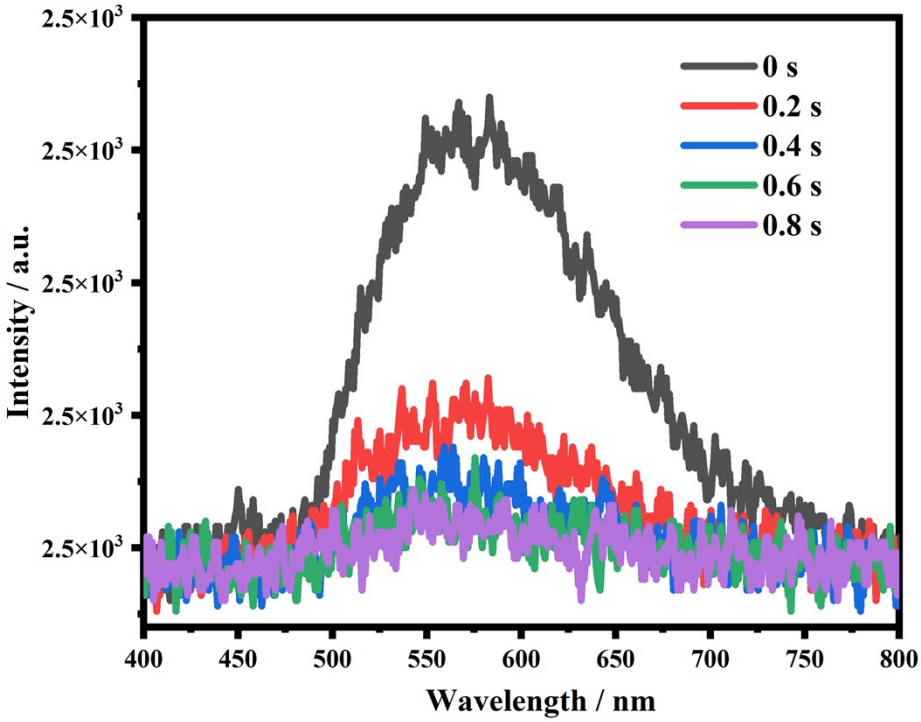

Figure S38. The time-resolved afterglow spectrum of **LIFM-ZJY-1** at 77 K under the 450 nm radiation.

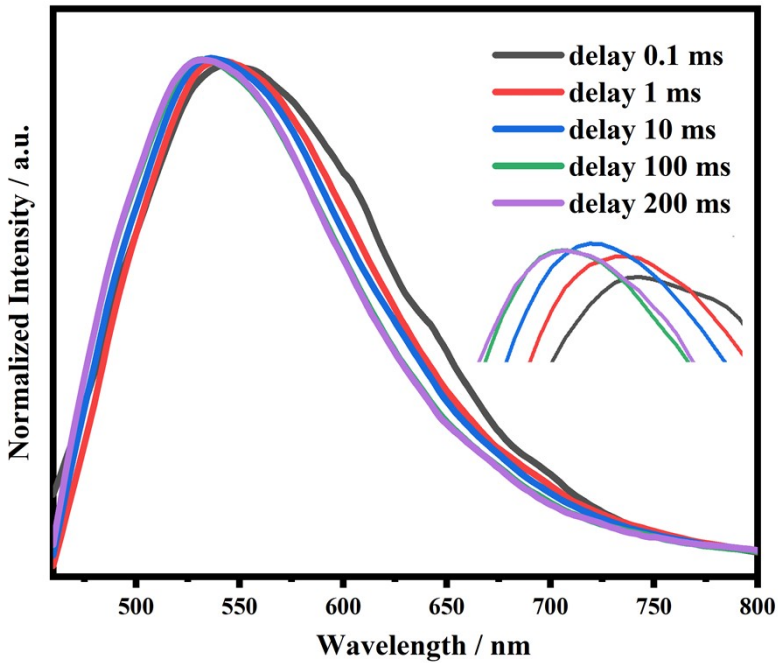

Figure S39. Normalized delayed emission spectra of **LIFM-ZJY-1** at 77 K with different delay times (λ_{ex} = 450 nm), and the inset shows the blue-shift of the emission peak with elongated delay times.

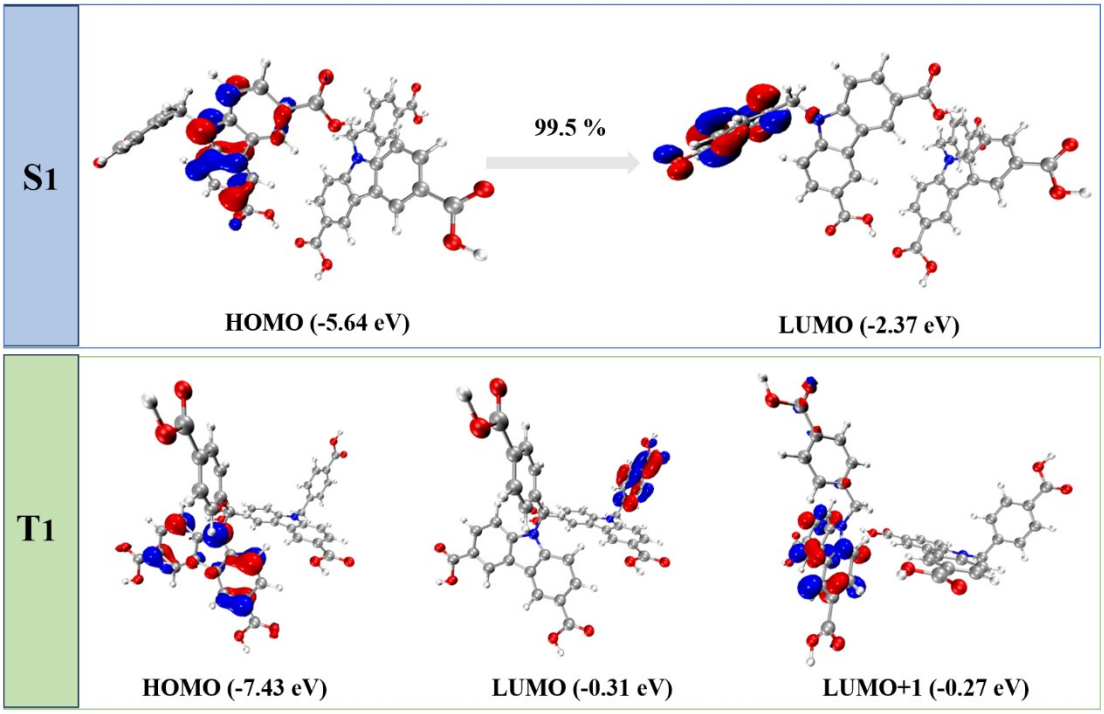

Figure S40. The electronic transition characters for S_1 (up) and T_1 (down) states and the dominant frontier molecular orbitals of L dimer at B3LYP /6-311G(d) level.

Table S1. Crystal data and structure refinement parameters for two compounds.

Compound	LIFM-ZJY-1	LIFM-ZJY-2
Formula	$C_{22}H_{12}CdNO_6$	$C_{44}H_{24}N_2O_{12}Zn_2$
Formula Weight	498.73	903.39
Crystal System	monoclinic	monoclinic
Space Group	$P2_1/c$	$P2_1$
T (K)	293.24(10)	240.01(10)
a (Å)	12.7379(3)	13.4886(3)
b (Å)	21.7172(4)	19.3470(4)
c (Å)	12.2909(2)	13.4988(2)
α (°)	90	90
β (°)	111.294(2)	115.605(2)
γ (°)	90	90
V(Å^3)	3167.93(11)	3176.74(12)
Z	4	2
ρ_{cal} (g/cm^3)	1.046	0.944
μ (mm^{-1})	5.743	0.798
Reflections collected	26294	80838

F(000)	988.0	916.0
Data / restraints / parameters	5421/0/271	22230/1/542
R1[I>2σ(I)]	R1 = 0.0279, wR2 = 0.0768	R1 = 0.0379, wR2 = 0.0941
wR2 (all data)/ GooF	R1 = 0.0328, wR2 = 0.0791	R1 = 0.0536, wR2 = 0.1027
CCDC number	2328844-	2328845

Table S2. The fluorescence lifetimes of **L** excited by 350 nm at RT.

wavelength	τ_1 / ns	A_1 / %	τ_2 / ns	A_2 / %	τ / ns	χ^2
394 nm	0.59	95.21	3.71	4.79	0.74	1.19
450 nm	1.80	74.29	7.28	25.71	3.21	1.19

Table S3. The phosphorescence lifetimes of **L** excited by 350 nm at RT.

wavelength	τ_1 /μs	A_1 / %	τ_2 /μs	A_2 / %	τ /μs	χ^2
560 nm	258.01	72.24	4205.09	27.76	1353.72	1.29

Table S4. The fluorescence lifetimes of **L** excited by 350 nm at 77 K.

wavelength	τ_1 / ns	A_1 / %	τ_2 / ns	A_2 / %	τ / ns	χ^2
394 nm	0.29	94.22	2.89	5.78	0.44	1.06

Table S5. The phosphorescence lifetimes of **L** excited by 350 nm at 77 K.

wavelength	τ_1 / ms	A_1 / %	τ_2 / ms	A_2 / %	τ / ms	χ^2
548 nm	11.14	51.14	175.81	48.86	91.60	1.19

Table S6. The fluorescence lifetimes of **LIFM-ZJY-1** excited by 350 nm at RT.

wavelength	τ_1 / ns	A_1 / %	τ_2 / ns	A_2 / %	τ / ns	χ^2
367 nm	0.34	90.94	3.50	9.06	0.62	1.15
386 nm	0.96	65.80	5.75	34.20	2.60	1.27
453 nm	3.42	77.62	12.27	22.38	5.41	1.29

Table S7. The phosphorescence lifetimes of **LIFM-ZJY-1** excited by 350 nm at RT.

wavelength	τ_1 /μs	A_1 / %	τ_2 /μs	A_2 / %	τ /μs	χ^2
540 nm	978.82	54.77	5309.15	45.23	2937.43	1.27

Table S8. The fluorescence lifetimes of **LIFM-ZJY-1** excited by 350 nm at 77 K.

wavelength	τ_1 / ns	A_1 / %	τ_2 / ns	A_2 / %	τ / ns	χ^2
376 nm	0.26	68.66	3.32	31.34	1.22	0.98
394 nm	1.46	55.03	4.58	44.97	2.86	1.10

Table S9. The phosphorescence lifetimes of **LIFM-ZJY-1** excited by 350 nm at 77 K.

wavelength	τ_1 / ms	A_1 / %	τ_2 / ms	A_2 / %	τ / ms	χ^2
468 nm	17.56	28.28	410.14	71.72	299.12	1.24
490 nm	113.84	36.74	973.05	63.26	657.38	1.26
532 nm	88.68	41.32	593.21	58.68	384.74	1.29
586 nm	25.57	30.96	318.13	69.04	227.55	1.27

Table S10. The fluorescence lifetimes of **LIFM-ZJY-2** excited by 350 nm at RT.

wavelength	τ_1 / ns	A_1 / %	τ_2 / ns	A_2 / %	τ / ns	χ^2

386 nm	2.37	55.19	5.19	44.81	3.63	1.15
394 nm	2.92	72.16	6.31	27.84	3.86	1.26
450 nm	2.82	80.65	9.04	19.35	4.02	1.26

Table S11. The phosphorescence lifetimes of **LIFM-ZJY-2** excited by 350 nm at RT.

wavelength	τ_1 / ms	A_1 / %	τ_2 / ms	A_2 / %	τ / ms	χ^2
528 nm	2.67	58.51	17.52	41.49	8.83	1.28

Table S12. The fluorescence lifetimes of **LIFM-ZJY-2** excited by 350 nm at 77 K.

wavelength	τ_1 / ns	A_1 / %	τ_2 / ns	A_2 / %	τ / ns	χ^2
386 nm	1.68	29.78	6.39	70.22	4.99	1.25
392 nm	4.01	54.87	8.57	45.13	6.08	1.25

Table S13. The phosphorescence lifetimes of **LIFM-ZJY-2** excited by 350 nm at 77 K.

wavelength	τ_1 / ms	A_1 / %	τ_2 / ms	A_2 / %	τ / ms	χ^2
476 nm	176.04	22.37	1415.83	77.63	1138.49	1.24
500 nm	282.33	24.27	1594.94	75.73	1276.37	1.28
546 nm	205.88	32.20	1315.71	67.80	958.34	1.28
589 nm	159.01	35.16	1037.58	64.84	728.67	1.26

Table S14. The absolute photoluminescence quantum yields (Φ_{total}) for three compounds at room temperature.

	L	**LIFM-ZJY-1**	**LIFM-ZJY-**

			2
RT	1.3 %	10.2 %	3.1 %
77 K	4.7 %	18.1 %	13 %

Table S15. TD-DFT calculated singlet energy levels of **L** monomer.

Excited State	Energy/eV	λ/nm	f	Transition configuration/%
S_1	2.79	445	0.00001	H→L (99.5)
S_2	3.30	376	0.00000	H-1→L (99.6)
S_3	3.98	312	0.04860	H→L+1 (48.3) H→L+2 (35.5) H-1→L+1 (7.6) H-1→L+2 (5.1)
S_4	4.03	307	0.10440	H→L+1 (37.6) H→L+2 (35.4) H-1→L+1 (15.3) H-1→L+2 (6.2)
S_5	4.17	297	0.00010	H-7→L (96.3)

Table S16. TD-DFT calculated triplet energy levels of **L** monomer.

Excited State	Energy/eV	λ/nm	Transition configuration/%
T_1	2.43	510	H→L (79.6) H-1→L+2 (8.1) H-8→L+5 (6.0)
T_2	3.35	370	H-2→L+1 (54.4) H-3→L+4 (26.4) H-4→L+1 (5.6) H-3→L+1 (5.1)
T_3	3.39	366	H-1→L (59.8) H-8→L (6.7)

			H-4→L+2 (5.7)
			H→L+5 (5.5)
			H→L+2 (5.3)
T_4	3.76	330	H→L+2 (66.5)
			H-1→L (16.9)
T_5	3.93	315	H-1→L+2 (58.1)
			H→L (16.4)
			H-4→L+3 (8.9)
T_6	4.00	310	H-1→L+3 (29.9)
			H-1→L (15.2)
			H→L+2 (14.6)
			H-4→L+2 (11.6)
			H→L+5 (9.2)
			H-8→L (7.8)

Table S17. The S_n/T_n spin-orbit coupling (SOC) constants (ξ) of **L** monomer.

S_n/T_n	ξ / cm^{-1}	S_n/T_n	ξ / cm^{-1}
S_0-T_1	1.42	S_3-T_1	1.45
S_0-T_2	0.79	S_3-T_2	0.78
S_0-T_3	0.78	S_3-T_3	3.16
S_0-T_4	9.48	S_3-T_4	0.47
S_0-T_5	4.71	S_3-T_5	1.36
S_1-T_1	3.46	S_4-T_1	1.45
S_1-T_2	1.31	S_4-T_2	0.65
S_1-T_3	1.66	S_4-T_3	1.84
S_1-T_4	2.18	S_4-T_4	0.37
S_1-T_5	0.22	S_4-T_5	0.80
S_2-T_1	3.06	S_5-T_1	2.90
S_2-T_2	1.24	S_5-T_2	5.33
S_2-T_3	2.28	S_5-T_3	0.74

S_2-T_4	1.14	S_5-T_4	0.43
S_2-T_5	0.74	S_5-T_5	0.34

Table S18. TD-DFT calculated singlet energy levels of **L** dimer.

Excited State	Energy/eV	λ/nm	f	Transition configuration/%
S_1	2.71	457	0.0001	H→L (99.5)
S_2	3.26	380	0.0000	H-1→L (99.6)
S_3	3.63	342	0.0001	H→L+1 (71.1) H→L+2 (28.4)
S_4	3.62	341	0.0000	H-2→L (100)
S_5	3.73	332	0.0000	H→L+2 (71.1) H→L+1 (28.7)
S_6	3.86	329	0.0242	H→L+3 (56.1) H→L+4 (34.3)

Table S19. TD-DFT calculated triplet energy levels of **L** dimer.

Excited State	Energy/eV	λ/nm	Transition configuration/%
T_1	2.32	535	H→L+1 (68.2) H→L+4 (13.2) H-2→L+2 (10.6)
T_2	2.62	472	H-2→L+1 (48.2) H→L+4 (15.3) H-2→L+2 (8.8) H-14→L+10 (5.6)
T_3	3.04	408	H-3→L+5 (36.2) H-1→L+3 (27.9) H-17→L+11 (5.7) H-3→L+6 (5.5)
T_4	3.29	377	H→L+1 (41.8)

			H-2→L+10 (10.0) H-8→L+4 (9.2) H→L+2 (6.3) H-14→L+1 (5.7)
T_5	3.34	371	H-4→L+2 (45.5) H-6→L+9 (26.0) H-4→L+1 (8.0)
T_6	3.33	370	H-5→L (46.6) H-7→L+8 (25.2) H-7→L (6.3) H-9→L (6.0) H-5→L+3 (5.2)

Table S20. The S_n/T_n spin-orbit coupling (SOC) constants (ξ) of **L** dimer.

S_n/T_n	ξ / cm^{-1}	S_n/T_n	ξ / cm^{-1}
S_0-T_1	0.50	S_3-T_1	0.85
S_0-T_2	1.24	S_3-T_2	0.12
S_0-T_3	1.18	S_3-T_3	0.19
S_0-T_4	1.01	S_3-T_4	0.32
S_0-T_5	1.72	S_3-T_5	0.33
S_1-T_1	0.29	S_4-T_1	0.25
S_1-T_2	0.27	S_4-T_2	0.08
S_1-T_3	0.99	S_4-T_3	0.21
S_1-T_4	0.17	S_4-T_4	0.50
S_1-T_5	0.48	S_4-T_5	0.10
S_2-T_1	0.40	S_5-T_1	0.30
S_2-T_2	0.34	S_5-T_2	0.05
S_2-T_3	0.19	S_5-T_3	0.39
S_2-T_4	0.14	S_5-T_4	0.16
S_2-T_5	0.54	S_5-T_5	0.05

References

1. Sheldrick, G. M., SHELXTL-97, Program for Crystal Structure Solution and Refinement. *University of Göttingen: Göttingen* **1997**.

2. Dolomanov, O. V.; Bourhis, L. J.; Gildea, R. J.; Howard, J. A. K.; Puschmann, H., OLEX2: A Complete Structure Solution, Refinement and Analysis Program. *Journal of Applied Crystallography* **2009,** *42* (2), 339.

3. Frisch, M. J.; Trucks, G. W.; Schlegel, H. B.; Scuseria, G. E.; Robb, M. A.; Cheeseman, J. R.; Scalmani, G.; Barone, V.; Mennucci, B.; Petersson, G. A.; Nakatsuji, H.; Caricato, M.; Li, X.; Hratchian, H. P.; Izmaylov, A. F.; Bloino, J.; Zheng, G.; Sonnenberg, J. L.; Hada, M.; Ehara, M.; Toyota, K.; Fukuda, R.; Hasegawa, J.; Ishida, M.; Nakajima, T.; Honda, Y.; Kitao, O.; Nakai, H.; Vreven, T.; Montgomery, J. A., Jr.; Peralta, J. E.; Ogliaro, F.; Bearpark, M. J.; Heyd, J.; Brothers, E. N.; Kudin, K. N.; Staroverov, V. N.; Kobayashi, R.; Normand, J.; Raghavachari, K.; Rendell, A. P.; Burant, J. C.; Iyengar, S. S.; Tomasi, J.; Cossi, M.; Rega, N.; Millam, N. J.; Klene, M.; Knox, J. E.; Cross, J. B.; Bakken, V.; Adamo, C.; Jaramillo, J.; Gomperts, R.; Stratmann, R. E.; Yazyev, O.; Austin, A. J.; Cammi, R.; Pomelli, C.; Ochterski, J. W.; Martin, R. L.; Morokuma, K.; Zakrzewski, V. G.; Voth, G. A.; Salvador, P.; Dannenberg, J. J.; Dapprich, S.; Daniels, A. D.; Farkas; Foresman, J. B.; Ortiz, J. V.; Cioslowski, J.; Fox, D. J., Gaussian 09. *Gaussian, Inc.: Wallingford, CT.* **2009**.

4. Gao, X.; Bai, S.; Fazzi, D.; Niehaus, T.; Barbatti, M.; Thiel, W., Evaluation of Spin-Orbit Couplings with Linear-Response Time-Dependent Density Functional Methods. *Journal of Chemical Theory and Computation* **2017,** *13* (2), 515.

5. Spackman, P. R.; Turner, M. J.; McKinnon, J. J.; Wolff, S. K.; Grimwood, D. J.; Jayatilaka, D.; Spackman, M. A., CrystalExplorer: a program for Hirshfeld surface analysis, visualization and quantitative analysis of molecular crystals. *J Appl Crystallogr* **2021,** *54* (Pt 3), 1006-1011.

6. Lu, T.; Chen, F., Multiwfn: A Multifunctional Wavefunction Analyzer. *Journal of Computational Chemistry* **2012,** *33* (5), 580.

7. Humphrey, W., Dalke, A. and Schulten, K., VMD:Visual. Molecular Dynamics, *J. Molec. Graphics* **1996,** 14.1, 33-38.